OXFORD
SOT | Society of Toxicology
academic.oup.com/toxsci

Toxicological Sciences, 2023, **191(1)**, 61–78
https://doi.org/10.1093/toxsci/kfac113
Advance Access Publication Date: 27 October 2022
Research article

Aerosol physicochemical determinants of carbon black and ozone inhalation co-exposure induced pulmonary toxicity

Nairrita Majumder,[1,2] Vamsi Kodali,[1,2,3] Murugesan Velayutham,[1,2,4] Travis Goldsmith,[1,2] Jessica Amedro,[1] Valery V. Khramtsov,[4] Aaron Erdely,[1,2,3] Timothy R. Nurkiewicz,[1,2,3] Jack R. Harkema,[5] Eric E. Kelley,[1,2,3] Salik Hussain[1,2,3,*]

[1]Department of Physiology and Pharmacology, School of Medicine, West Virginia University, Morgantown, West Virginia 26506, USA,
[2]Center for Inhalation Toxicology (iTOX), School of Medicine, West Virginia University, Morgantown, West Virginia 26506, USA, ,
[3]Health Effects Laboratory Division, National Institute for Occupational Safety and Health (NIOSH), Morgantown, West Virginia 26508, USA,
[4]Department of Biochemistry and Molecular Medicine, School of Medicine, West Virginia University, Morgantown, West Virginia 26506, USA and
[5]Department of Pathobiology and Diagnostic Investigation, College of Veterinary Medicine, Michigan State University, East Lansing, Michigan 48824, USA

Nairrita Majumder and Vamsi Kodali contributed equally to this study.

Disclaimer: The findings and conclusions in this report are those of the author(s) and do not necessarily represent the official position of the National Institutes of Health and National Institute for Occupational Safety and Health, Centers for Disease Control and Prevention. Mention of brand name does not constitute product endorsement.

*To whom correspondence should be addressed at Department of Physiology and Pharmacology, Center for Inhalation Toxicology (iTOX), School of Medicine, West Virginia University, Morgantown, WV 26506, USA. E-mail: salik.hussain@hsc.wvu.edu.

Abstract

Air pollution accounts for more than 7 million premature deaths worldwide. Using ultrafine carbon black (CB) and ozone (O_3) as a model for an environmental co-exposure scenario, the dose response relationships in acute pulmonary injury and inflammation were determined by generating, characterizing, and comparing stable concentrations of CB aerosols (2.5, 5.0, 10.0 mg/m^3), O_3 (0.5, 1.0, 2.0 ppm) with mixture CB + O_3 (2.5 + 0.5, 5.0 + 1.0, 10.0 + 2.0). C57BL6 male mice were exposed for 3 h by whole body inhalation and acute toxicity determined after 24 h. CB itself did not cause any alteration, however, a dose response in pulmonary injury/inflammation was observed with O_3 and CB + O_3. This increase in response with mixtures was not dependent on the uptake but was due to enhanced reactivity of the particles. Benchmark dose modeling showed several-fold increase in potency with CB + O_3 compared with CB or O_3 alone. Principal component analysis provided insight into response relationships between various doses and treatments. There was a significant correlation in lung responses with charge-based size distribution, total/alveolar deposition, oxidant generation, and antioxidant depletion potential. Lung tissue gene/protein response demonstrated distinct patterns that are better predicted by either particle dose/aerosol responses (interleukin-1β, keratinocyte chemoattractant, transforming growth factor beta) or particle reactivity (thymic stromal lymphopoietin, interleukin-13, interleukin-6). Hierarchical clustering showed a distinct signature with high dose and a similarity in mRNA expression pattern of low and medium doses of CB + O_3. In conclusion, we demonstrate that the biological outcomes from CB + O_3 co-exposure are significantly greater than individual exposures over a range of aerosol concentrations and aerosol characteristics can predict biological outcome.

Keywords: ozone; ultrafine carbon black; physicochemical properties; inhalation; co-exposure; inflammation

Inhalation co-exposure to ultrafine particulate and gaseous components of air pollution represent more realistic exposure scenario compared with individual particulate or gaseous exposures. The World Health Organization (WHO) attribute air pollution to be associated with approximately 7 million premature deaths per year making it one of the top 5 causes of mortality (World Health Organization, 2016). A significant increase in morbidity, hospitalizations, and economic losses (lost workdays) are also associated with air pollution (Birnbaum *et al.*, 2020). In the past year, approximately 160 million individuals in the United States breathe air exceeding federal air quality standards (GBDCRD, 2017; GBDRFC, 2016). These levels, although lower than many more polluted areas of the world, are still effective in exacerbating cardio-respiratory and other systemic conditions in vulnerable populations (GBDCRD, 2017; GBDRFC, 2016). Both short- and long-term exposure to particulate matter significantly increase mortality, morbidity, and hospitalization rates (Anenberg *et al.*, 2014; Apte *et al.*, 2015). Over the last decade, WHO's Air Pollution Health Risk Assessment (AP-HRA) and a significant body of literature have positively associated the major pollutants like ozone (O_3) and particulate matter to cardiopulmonary, systemic, reproductive, as well as cognitive disorders (Campen *et al.*, 2009; Cleary *et al.*, 2018; Ghosh *et al.*, 2021; Shehab and Pope, 2019).

Graphical abstract

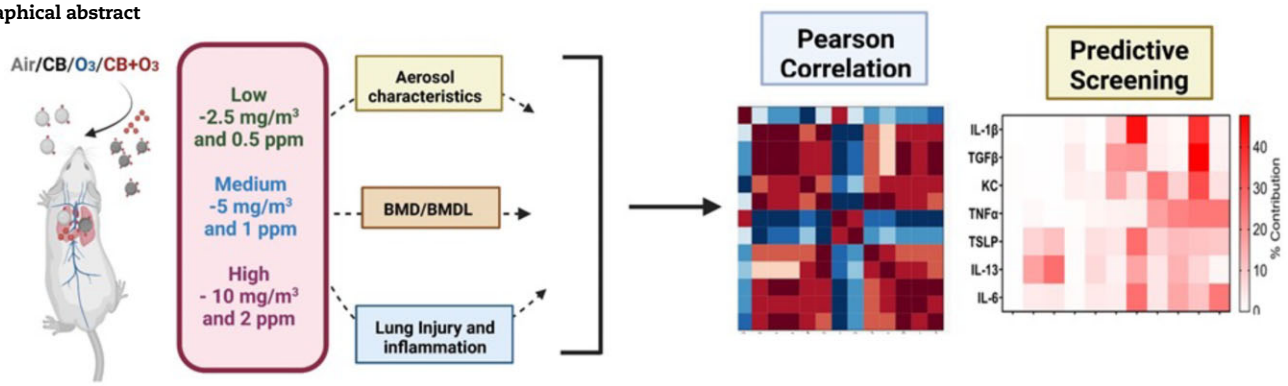

Epidemiological data suggest a positive association between co-exposure to particulate matter and gases to pulmonary complication related hospitalization rates (Rhee, 2018). A growing body of evidence suggest interactive effects of exposure to different types of particulates and gases including O_3, NO_2, and volatile organic compounds (Mauderly and Samet, 2009). Co-exposure to particulate matter and O_3 has already been linked to aggravated cardiovascular outcomes, exacerbated lung injury in pre-existing cardiovascular disease and increased airway and systemic inflammation in elderly subjects (Hamade *et al.*, 2008, 2010; Holz *et al.*, 2018; Wagner *et al.*, 2014; Wong *et al.*, 2018).

We recently described an ultrafine carbon black (CB) and O_3 inhalation co-exposure model to more accurately replicate particle and gases mixed exposures (Hathaway *et al.*, 2021; Majumder *et al.*, 2021a,b). Ground level O_3 is one of the most reactive components of air pollution and is classified as a criteria pollutant by the U. S. Environmental Protection Agency (US EPA). Epidemiological and clinical studies confirm a strong association between short term acute exposure to O_3 and exacerbation of pre-existing lung conditions in vulnerable population (Farhat *et al.*, 2013; Fauroux *et al.*, 2000; Yang *et al.*, 2003). The EPA estimate a linear relationship between O_3 and global warming, anticipating an approximately 14% increase in O_3 associated mortality level across the globe by 2030 (Wilson *et al.*, 2017). CB is a significant occupational and environmental health hazard, with a wide range of application as a reinforcing agent in rubber, paints, and in leather industries (Pirela *et al.*, 2017; Rattanasom *et al.*, 2007; Singh *et al.*, 2022). Occupational exposure to CB is associated with inflammation and decline in lung function (Harber *et al.*, 2003; Zhang *et al.*, 2014).

Previous studies on particulate matter as well as nanoparticles clearly underpin the role of physicochemical characteristics in dictating the biological activity of the particulates (Braakhuis *et al.*, 2014; Hussain *et al.*, 2009, 2010; Nurkiewicz *et al.*, 2008; Shin *et al.*, 2015). Although this phenomenon is well known for the ultrafine/nanoparticles, the relative contribution/association of different aerosol characteristics with biological activity in case of ultrafine CB and O_3 mixed exposure is not known. Further, more computational approaches to predict biological activity based on aerosol characteristics are clearly needed to help hazard identification/risk assessment of an ever-growing number of aerosols. The purpose of this study was to elaborate the relationship between different aerosol physicochemical characteristics, oxidative properties, and uptake with pulmonary injury and inflammation using 3 different exposure levels. Apart from the multivariate analysis, we also used predictive screening (boot strap forest) to determine the relative contribution of these characteristics in co-exposure induced inflammatory protein secretions. We hypothesized that the contribution of differential macrophage uptake and alteration in physicochemical characteristics play important role in co-exposure induced increased biological activity.

Materials and methods

Exposure system, aerosol generation, and characterization

Whole-body inhalation exposures were conducted at various concentrations of CB aerosols (2.5, 5.0, 10.0 mg/m^3), O_3 gas (0.5, 1.0, 2.0 PPM) or mixtures of the 2 toxicants (2.5 CB/0.5 O_3, 5.0 CB/1.0 O_3, 10.0 CB/2.0 O_3). The exposure system has been detailed previously (Hathaway *et al.*, 2021; Majumder *et al.*, 2021a,b). Briefly, bulk CB material (Printex 90, provided as a gift from Evonik, Frankfurt, Germany) was aerosolized with a high-pressure acoustical generator (HPAG, IEStechno, Morgantown, West Virginia) then further deagglomerated with a venturi pump (JS-60M, Vaccon, Medway, Massachusetts) attached to the output of the generator. A light scattering device (pDr-1500, Thermo Environmental Instruments Inc, Franklin, Massachusetts) was used to estimate the mass concentration of the aerosol. O_3 gas was generated (HTU500AC, Ozone Solutions, Hull, Iowa) and mixed with the CB aerosol and fed into a stainless-steel exposure chamber (Cube 150, IEStechno). Chamber O_3 levels were measured with a calibrated monitor (Model 202, 2B Technologies, Inc, Boulder, Colorado). O_3 monitor calibration was independently verified using calorimetric O_3 gas detector tubes (Sensidyne LP, St Petersburgh, Florida). Mice were individually housed in stainless-steel mesh cages within the chamber and the temperature (20–22°C) and humidity (50–70%) were monitored and maintained within accepted animal comfort levels during exposures. Gravimetric measurements were conducted with 37 mm PTFE filters to report exposure mass concentrations and to continually calibrate the pDr-1500. The CB and O_3 levels were kept at constant, user-defined levels during exposures with automated feedback loops. Particle size distributions of the CB aerosol were periodically sampled from the exposure chamber with (1) an electrical low-pressure impactor (ELPI+, Dakati, Tempera, Finland); (2) an aerosol particle sizer (APS 3321, TSI Inc, Shoreview, Minnesota); and (3) a scanning mobility particle sizer (SMPS 3938, TSI Inc). Elemental composition at CB and CB + O_3 particle surfaces was analyzed using X-Ray Photo Electron Spectroscopy (XPS) technique using Physical electronics PHI 5000 Versa Probe XPS/UPS.

Lung histopathology

The non-lavaged lungs were fixed by tracheal instillation of 10% neutral buffered formalin. Fixed tissue was processed for light microscopy. Random transverse tissue blocks from the left lung lobes were paraffin embedded, sectioned at a thickness of 5 μg and stained with hematoxylin and eosin (H&E). Severity of exposure-related lung lesions were semi-quantitively scored via light microscopic examination, by a board-certified veterinary pathologist (J.R.H.) in a blinded manner (no knowledge of individual exposure conditions). Criteria-based scores for specific airway (bronchioles/alveolar duct) lesions (inflammation, epithelial necrosis/exfoliation/loss, monocyte/macrophage hyperplasia) were 0, no histopathology; 1, minimal, <10% of airway tissue affected; 2, mild, 10% < 25% airway tissue affected; 3, moderate, 25% < 50% airway tissue affected; 4, marked, 50% < 75% airway tissue affected; 5, severe, 75–100% airway tissue affected.

Electron paramagnetic resonance spectroscopic studies

Electron paramagnetic resonance (EPR) spin probe 1-hydroxy-3-carboxymethyl-2,2,5,5-tetramethyl-pyrrolidine (CMH; Enzo Life Sciences, Farmingdale, New York) was used to quantify the oxidant potential of CB particles collected from exposure chamber in the presence or absence of O_3. The particles (CB, CB + O_3– 10.0 mg/m^3 + 2.0 ppm, 5.0 mg/m^3 + 1.0 ppm, and 2.5 mg/m^3 + 0.25 ppm) were suspended at a concentration of 50 μg/ml in a cell culture grade sterile PBS (treated with Chelex 100), followed by incubation for 30 min at 37°C with 200 μM CMH. The serum samples were collected after exposure to CB particles with and without O_3 at different concentrations and were incubated with 200 μM CMH spin probe for 30 min at 37°C. The samples were flash frozen in liquid nitrogen and stored at −80°C for further quantification. Bruker EMXnano spectrometer (Bruker BioSciences, Billerica, Massachusetts) was used to measure the EPR active CM• radical which was formed due to the oxidation of CMH by the oxidative species on the surface of the CB particles.

At the time of EPR measurements, liquid samples were thawed and loaded (50 μl) into glass capillary tubes that were sealed on one end using Critoseal clay and placed inside a 4 mm (OD) EPR quartz tube. The quartz tube was positioned inside the resonator/cavity and EPR spectra were recorded at room temperature. The following EPR instrument settings were used: microwave frequency, 9.615 GHz; sweep width, 100 G; microwave power, 20 mW; modulation amplitude, 1 G; modulation frequency, 100 kHz; receiver gain, 50 dB; time constant, 10.24 ms; conversion time, 30 ms, sweep time, 30 s; number of scans, 1.

Ferric reducing ability of serum assay

The ferric reducing ability of serum (FRAS) assay solution was prepared as described previously (Majumder *et al.*, 2021a). FRAS assay was used to screen the acellular oxidant potential of the particles by quantifying the particulate capacity for antioxidant depletion. Serum is a rich source of various types of antioxidants. The antioxidant depletion potential of CB and CB + O_3 particles was measured by reacting human serum (Sigma Aldrich, St Louis, Missouri) with particles (CB, CB + O_3– 10.0 mg/m^3 + 2.0 ppm, 5.0 mg/m^3 + 1.0 ppm and 2.5 mg/m^3 + 0.5 ppm) at a concentration of 5.0 mg/ml, followed by sonication and incubation in a shaker at 450 RPM at 37°C for 3 h. The particles were separated after the incubation by centrifugation at 14,000 g for 30 min. This was followed by addition of 50 μl of serum to 1 ml of FRAS solution, as described previously (Majumder *et al.*, 2021b). The formation of blue color in the solution due to ferrous-tripyridyltriazine complex was measured at 586 nm wavelength in Spectramax iD5 plate reader. The reduction in the antioxidant capacity of serum was quantified and reported as percentage change with respect to control human serum.

Inhalation exposures

All animal procedures were approved by the WVU Institutional Animal Care and Use Committee (IACUC). C56BL/6J male mice (8 weeks old) were purchased from Jackson Laboratory (Bar Harbor, Maine) and acclimated at AAALAC accredited animal facility at the West Virginia University Health Sciences Center. All animals were maintained in a room with a 12-h light/dark cycle and provided chow and water *ad libitum*. Mice were randomly divided and exposed to filtered air, 3 different doses of either CB (10.0, 5.0, and 2.5 mg/m^3), or O_3 (2.0, 1.0, and 0.5 ppm and mixture) (CB + O_3) (10.0 mg/m^3 + 2.0 ppm, 5.0 mg/m^3 + 1.0 ppm, and 2.5 mg/m^3 + 0.5 ppm) for 3 h. These concentrations were referred to as low, medium, and high as presented in Table 1. Animals were euthanized 24 h post-exposure by intraperitoneal injection of Fatal Plus (pentobarbital sodium, 250 mg/kg).

Bronchoalveolar lavage fluid collection and analyses

Bronchoalveolar lavage fluid (BALF) was collected and quantified as previously described (Hathaway *et al.*, 2021; Majumder *et al.*, 2021a,b). Briefly, 1 ml of cold sterile PBS was instilled through the trachea and collected. The process was repeated 3 times to collect approximately 3 ml of BALF. Total cell number was determined using automated counter Countess II (Invitrogen, Waltham, Massachusetts). The cells were centrifuged at 600 rpm at 4°C for 5 min and the supernatant was collected and store at −80°C for further analysis (enzyme linked immunosorbent assay [ELISA], BCA, and dehydrogenase cytotoxicity [LDH] assay). The pelleted cells were resuspended in PBS, and slides were prepared by Cytospin (Thermo Fisher Scientific, Waltham, Massachusetts) for differential counts. Slides were stained with Hema 3 (Fisher Scientific, Pittsburgh, Pennsylvania) for the differential count analysis. The total protein content in the BALF was quantified using the Pierce BCA Assay kit (Thermo Fisher Scientific) as per the manufacturer's instructions. The LDH assay was performed using the LDH Assay Kit (Promega, Madison, Wisconsin) as per the manufacturer's instructions.

Lung function measurement

The lung function measurements were performed 24 h post-exposure using Scireq Flexivent mechanical ventilator system (SCIREQ, Inc, Montreal, Canada) as described by us previously (Majumder *et al.*, 2021b). The data were recorded using the FlexiWare v8.0 software. Briefly, the mouse was anesthetized with urethane (2 mg/kg), tracheotomized with tracheal cannula (18 gauge, 0.3 cmH_2O.s/ml resistance) and mechanically ventilated at 150 breaths/min, tidal volume of 10 ml/kg and a positive end-expiratory pressure of 3 cm H_2O. After 2 deep inflations (30 cmH_2O pressure), the baseline lung function parameters were measured by applying a broadband forced oscillation waveform (matched to the animal breathing frequency). Data were fitted to a single compartment or constant phase model to obtain the Total Respiratory System Resistance (Rrs) and dynamic compliance (Crs). The Forced Expiratory Volume at 0.1 s (FEV0.1) was measured in triplicates using the NPFEE extension for Flexivent.

Table 1. Exposure design for the study

	Treatment	Target Concentration
Low	Carbon black	2.5 mg/m^3
	Ozone	0.5 ppm
	Carbon black + ozone	2.5 mg/m^3 + 0.5 ppm
Medium	Carbon black	5 mg/m^3
	Ozone	1 ppm
	Carbon black + ozone	5 mg/m^3 + 1 ppm
High	Carbon black	10 mg/m^3
	Ozone	2 ppm
	Carbon black + ozone	10 mg/m^3 + 2 ppm

Target exposure concentration for low, medium, and high dose of carbon black (CB), ozone (O_3), and carbon black + ozone (CB + O_3).

Particle uptake by macrophages

Uptake of CB and CB + O_3 particles in the lavage macrophages was assessed to study the extent of interaction between macrophages and particles. This interaction was assessed in terms of (1) % of CB (black aggregates) positive lavage mononuclear cells and (2) amount of CB uptake (area of the cell occupied by the CB aggregates). At least 500 cells were counted to calculate % CB positive macrophages. Lavage cells (10,000) were spun on slides using Cytospin (Thermo Fisher Scientific) for differential counts and stained with Hema 3 (Fisher Scientific). Slides were allowed to dry and coverslips were applied before imaging. A total of 150 cells were imaged for each mouse (approximately 10 images per slide) to calculate the area of cell occupied by CB particles (Franca *et al.*, 2011). In total, 5 mice/slides were analyzed from each treatment group. Each slide was imaged multiple times scanning from bottom to top using Olympus AX70 Microscope (Japan) at 40× magnification. The area of particle uptake in macrophages was analyzed using the ImageJ Fiji software as described previously (Kulkarni *et al.*, 2005). The images were first deconvoluted by using the "Color Deconvolution" function. The images were converted into 8-bit grayscale and then converted into binary images by adjusting the threshold to include the black particles area. The area parameter was analyzed using the "Analyze Particle" function. The total area of the particle positive macrophages was estimated by converting the images to binary images and adjusting the threshold to capture the total cell area in the image. The ROI manager was used to include only the particle positive macrophages for the analysis. The data were reported and compared as a percentage of area covered by particles in macrophages.

Real-time PCR gene expression

The lung tissues were flash frozen in liquid nitrogen and pulverized over dry ice. The lung tissue powder was further used for RNA extraction and real-time PCR analysis. The RNA extraction was performed using Qiagen Rneasy Mini Kit (Qiagen, Germantown, Maryland) per the manufacturer's recommendations (Qiagen). The RNA concentration and purity were measured using Nanodrop. Reverse transcription was performed using the High-Capacity cDNA Reverse Transcription Kit (Thermo Fisher Scientific), following the manufacturer's recommendation. The Real-Time PCR was performed using AriamaX Real-time PCR System (Agilent, Santa Clara, California). The relative expression levels were normalized to 18 s housekeeping gene using Aria Real-Time PCR Software. Primer sequences are detailed in Supplementary Table 1.

Enzyme linked immunosorbent assay

Enzyme linked immunosorbent assay (ELISA) was performed on the BALF and lung tissue homogenate to quantify keratinocyte chemoattractant (KC), tumor necrosis factor-α (TNF- α), interleukin-6 (IL-6), interleukin-13 (IL-13), interleukin-1β (IL-1β), and thymic stromal lymphopoietin (TSLP) using the Duoset sandwich ELISA assay kits (R&D Systems, Minnesota) according to the manufacturer's recommendations. The absorbance was read at 450 nm wavelength in Spectramax iD5 plate reader. Lower limit of detection for these assays were IL-1β (15.6 pg/ml), TNF-α (31.3 pg/ml), KC (15.6 pg/ml), IL-6 (15.6 pg/ml), IL-13 (62.5 pg/ml), and TSLP (15.6 pg/ml).

Lung burden quantification

The lung burden at 24 h post-CB and/or CB + O_3 exposure was quantified 24 h after a single exposure following a previously published protocol (Elder *et al.*, 2005). Briefly, lungs were kept in a solution of 25% KOH/methanol (wt/vol) at 60°C heated block overnight, followed by centrifugation. The liquid was carefully decanted and the pellets were resuspended in equal volumes of nitric acid and methanol and kept at 60°C heated block for 3 h. This was followed by centrifugation, careful decantation of the supernatants, and resuspension of the pellet in 1 ml of 10% NP-40. The standard curve was made using particles and 10% NP-40. The absorbance was measured at 700 nm wavelength.

Hydrogen peroxide (H_2O_2) quantification

The H_2O_2 levels in lung homogenate and serum was quantified using the Amplex Red Hydrogen Peroxide/Peroxidase Assay Kit (Thermo Fisher Scientific). The lung tissues were flash frozen and pulverized over dry ice followed by lysis using RIPA buffer and 1% protease inhibitor cocktail. The protein extracted from lung tissue and serum samples was reacted with HRP and the Amplex Red dye for 45 min at room temperature in dark. The H_2O_2 reacts with the Amplex red dye to form a red fluorescent oxidation product, resorufin. The H_2O_2 levels were quantified by measuring the absorbances at 560 nm wavelength using SpectraMax iD5 plate reader (Molecular Devices, California). The obtained values were normalized to the protein content in the tissue using the Pierce BCA Assay Kit (Thermo Fisher Scientific) (Kunovac *et al.*, 2019).

Statistics

Data are presented as mean ± standard error of mean (SEM) unless mentioned otherwise. Normality of data was determined using either D'Agostino-Person and Shapiro-Wilk test. Statistical differences were calculated using either 1-way or 2-way Analysis of Variance (ANOVA) followed by Tukey's post hoc test, or a non-parametric ANOVA followed by Kruskal-Wallis post hoc test using GraphPad Prism 8.3 (GraphPad Software, San Diego, California). Differences between groups were considered significant when $p \leq .05$. Differences between control and exposed groups are denoted by *, whereas difference between treated groups at the same dose are denoted by #. United States Environmental Protection Agency's Benchmark Dose Software (BMDS) Version 3 (US EPA, 2022) was used to evaluate the Benchmark dose (BMD) response (Filipsson *et al.*, 2003; Haber *et al.*, 2018). The Akaike Information Criterion (AIC) was used for model selection, and the model with the lowest AIC value was used to select the best model between the various models. A change in 1 standard deviation (SD) in response rate was used as the benchmark response (BMR). Multivariate analysis including pairwise regression analysis, Pearson's correlation (r), non-parametric spearman's (ρ), hierarchical clustering analysis (HCA), and principal component analysis (PCA) were

performed using JMP version 13 (SAS institute, Cary, North Carolina) (Jolliffe and Cadima 2016; Ringner 2008). Predictive screening was performed using Boot Strap Forest approach (Klimberg and McCullough, 2016). The % contribution from the screening was plotted as a heat map. To avoid the use of laboratory animals for unnecessary duplication of our own recently published information, including published cell count data for only the highest dose group (Table 3) (Hathaway *et al.*, 2021; Majumder *et al.*, 2021a) was used for meta-analysis. Lung tissue gene expression and BALF protein expression assays for the highest dose group were performed again on a pool of banked samples from these studies.

Results

Aerosol characteristics

Realtime monitoring, size distributions, and depositions

Aerosol size distributions were estimated by real-time monitoring which confirmed stable aerosol generation at all exposure levels (Figure 1A). We previously published detailed analyses on aerosol morphology using transmission and scanning electron microscopy (Hathaway *et al.*, 2021; Majumder *et al.*, 2021a,b). APS-SMPS concurrent measurements (mobility-based quantification) as well as ELPI+ (charge-based measurements) confirmed that CB and CB + O_3 aerosols were not very different and were mainly composed of nano/ultrafine particles. Size distributions are

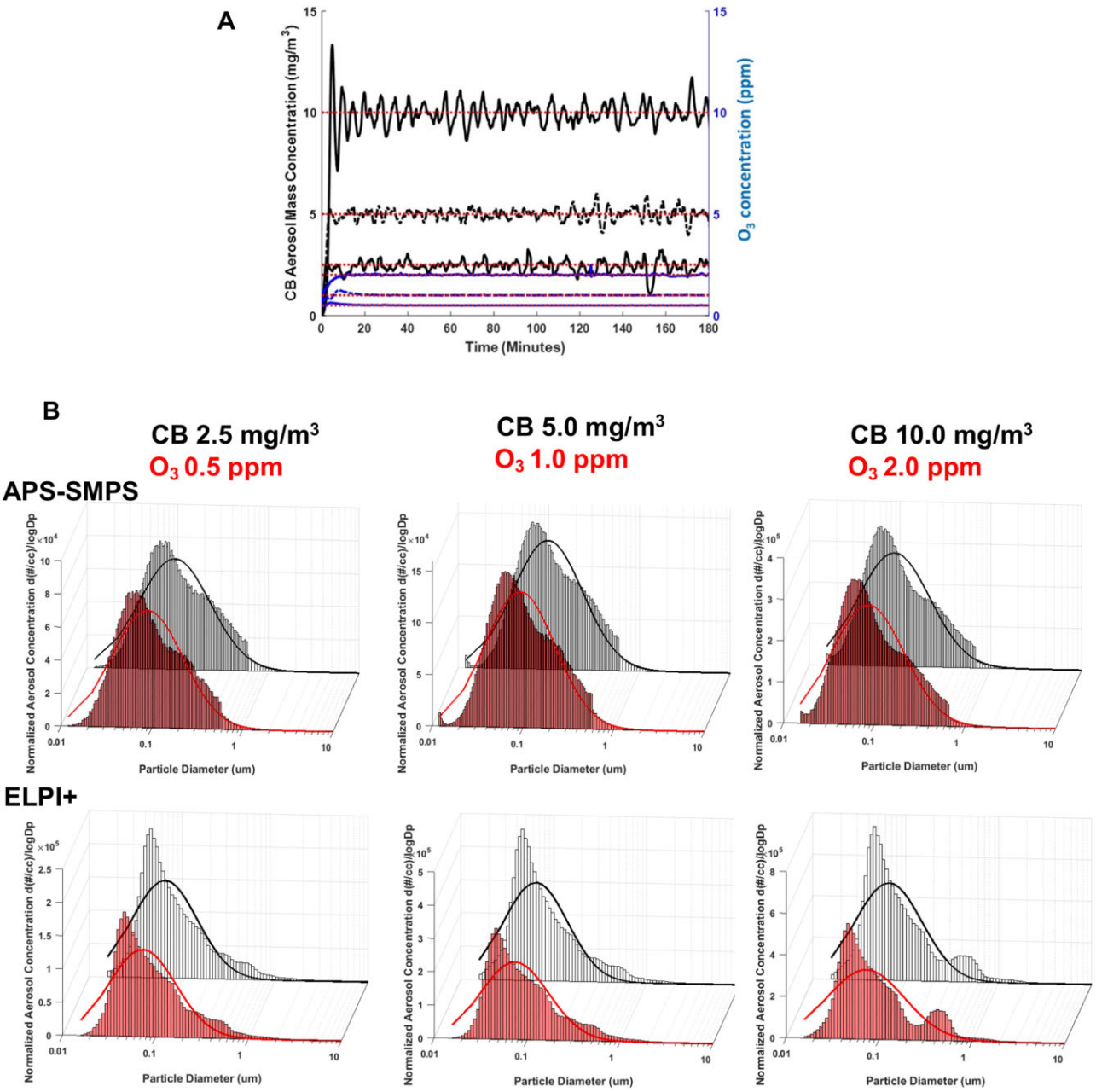

Figure 1. Aerosol exposure and characterization. A, Real-time monitoring of CB and O_3 levels during different exposures. B, Aerosol size distribution of CB (2.5, 5.0, and 10.0 mg/m^3) and CB + O_3 (2.5 mg/m^3 + 0.5 ppm, 5.0 mg/m^3 + 1.0 ppm, 10.0 mg/m^3 + 2.0 ppm) aerosol particles collected from the inhalation exposure chamber using an aerosol particle sizer (APS) in combination with scanning mobility particle sizer (SMPS) and an electrical low-pressure impactor (ELPI+).

Table 2. Aerosol distributions and deposition calculations

	SMPS/APS CMD nm (GSD)	SMPS/APS #/cc	ELPI+CMD nm (GSD)	ELPI+#/cc	Alveolar Deposited Dose (μg) (MPPD)	Total Deposited Dose (μg) (MPPD)
CB 2.5 mg/m^3	92.3 (2.47)	0.66E+05	64.8 (2.23)	1.27E+05	1.17	2.33
CB 2.5 mg/m^3 + O_3 0.5 ppm	89.7 (2.46)	0.70E+05	72.6 (2.29)	1.19E+05	1.23	2.42
CB 5.0 mg/m^3	97.1 (2.42)	1.20E+05	63.6 (2.19)	2.54E+05	2.46	4.87
CB 5.0 mg/m^3 + O_3 1.0 ppm	93.0 (2.44)	1.28E+05	73.9 (2.31)	2.13E+05	2.47	4.87
CB 10.0 mg/m^3	85.8 (2.48)	2.72E+05	65.2 (2.28)	4.22E+05	4.92	9.68
CB 10.0 mg/m^3 + O_3 2.0 ppm	85.7 (2.49)	2.89E+05	72.5 (2.59)	3.48E+05	4.82	9.54

Count median diameters (CMD) and geometric standard deviations (GSD) calculations at the indicated exposure concentrations from CB and CB + O_3 using SMPS/APS and ELPI+. Total lung and alveolar deposition estimates using multiple path particle dosimetry (MPPD) software at the end of exposure without accounting for clearance.

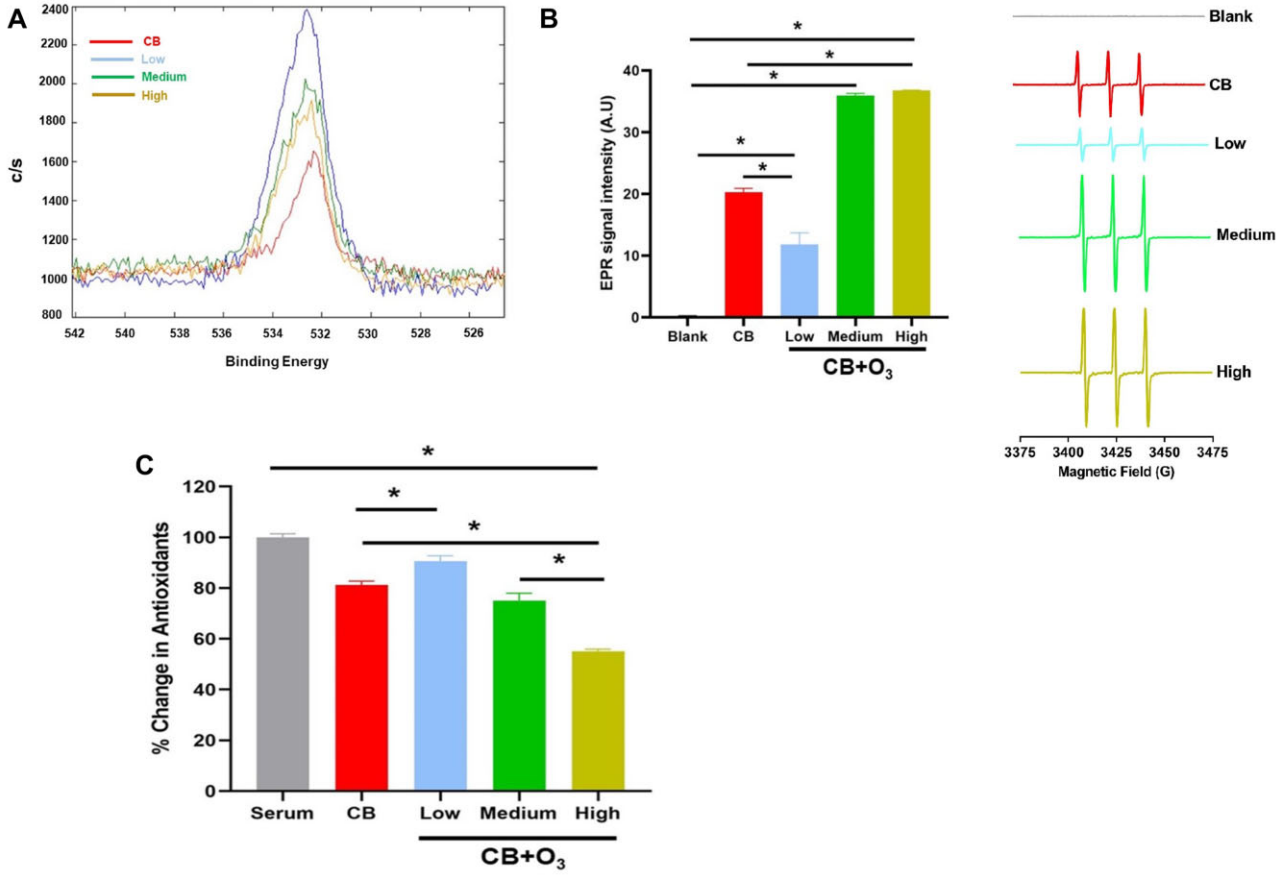

Figure 2. Acellular characterization of aerosol reactivity. A, XPS analysis representing surface oxygen contents of CB and CB + O_3 particles at low (2.5 mg/m^3 + 0.5 ppm), medium (5 mg/m^3 + 1 ppm) and high (10 mg/m^3 + 2 ppm) dose. B, Representative X-band electron paramagnetic resonance (EPR) spectra of CM• in PBS with single (CB) and co-exposure (CB + O_3) particles suspension (50 μg/ml) at low (2.5 mg/m^3 + 0.5 ppm), medium (5 mg/m^3 + 1 ppm), and high (10 mg/m^3 + 2 ppm) dose. Histogram represents intensity of the first peak of EPR signals. C) FRAS assay of single (CB) and co-exposure (CB + O_3) aerosol at low (2.5 mg/m^3 + 0.5 ppm), medium (5 mg/m^3 + 1 ppm), and high (10 mg/m^3 + 2 ppm) exposure dose. Data are presented as mean ± SEM of 3 independent experiments. Data analyzed by 1-way ANOVA followed by Tukey's post hoc test. *$p < .05$.

presented in Figure 1B, whereas measured count median diameter and geometric SD are presented in Table 2. Particle number concentrations show a clear dose dependent increase. For low medium and high exposures, multiple path particle dosimetry (MPPD) model predicted 2.33, 4.87, and 9.68 μg deposition for CB and 2.42, 4.87, and 9.54 μg total deposited dose for CB + O_3, respectively. Gravimetric estimates (from particles collected onto a filter inside the inhalation exposure chamber) confirmed aerosol concentrations remained within 5% of the target levels.

Surface characterization and oxidative potentials

Surface oxygen content measurement by XPS confirmed higher amount of surface oxygen in the case of CB + O_3 (for all the test doses) compared with CB (Figure 2A). Particles in pristine CB aerosol had 3.5% surface oxygen content, while low, medium, and high co-exposure aerosol particles had 8.6%, 5.4%, and 5.2% surface oxygen content. Aerosol ability to generate oxidants was evaluated by EPR using spin probe CMH which confirmed highest oxidant generation by the medium and high concentrations,

Table 3. Pulmonary injury and inflammation.

	BALF Total Cell ($\times 10^5$)	BALF Macrophages ($\times 10^5$)	BALF PMN ($\times 10^5$)	BALF LDH (Fold Change to Air)	BALF Total Protein (mg/ml)	Tissue H_2O_2 (nM)	Serum H_2O_2 (μM)	Serum Oxidants EPR (Arb. Units)	Respiratory Resistance ($cmH_2O.s/ml$)	Dynamic Compliance (ml/cmH_2O)	Forced Expiratory Volume (0.1) (ml)
Air	6.1 ± 1.9	6.1 ± 1.9	0 ± 0	1.00 ± 0.3	87.5 ± 22.7	57.3 ± 15.5	1.08 ± 0.19	2.91 ± 0.41	0.6 ± 0.11	0.037 ± 0.001	1.0 ± 0.06
CB Low	6.4 ± 0.8	6.4 ± 0.8	0 ± 0	2.84 ± 0.9	116.6 ± 25.4	61.6 ± 13.6	1.46 ± 0.22	2.94 ± 0.49	0.6 ± 0.01	0.032 ± 0.004	0.93 ± 0.03
CB Med	5.8 ± 1.8	5.8 ± 1.8	0 ± 0	1.19 ± 0.1	83.9 ± 17.7	93.7 ± 36.5	1.69 ± 0.13	2.62 ± 1.53	0.6 ± 0.03	0.037 ± 0.004	0.89 ± 0 .11
CB High	6.3 ± 1.5	6.3 ± 1.5	0 ± 0	0.50 ± 0.1	82.02 ± 10.0	75.2 ± 41.2	1.38 ± 0.75	2.13 ± 0.77	0.7 ± 0.08	0.035 ± 0.001	0.92 ± 0.02
O_3 Low	9.2 ± 4.3	9.1 ± 4.3	0.1 ± 0.1	1.58 ± 0.7	228.4 ± 49.2*	66.7 ± 16.7	1.68 ± 0.19*	2.91 ± 0.40*	0.6 ± 0.02	0.034 ± 0.003	0.94 ± 0.03
O_3 Med	9.1 ± 2.6	8.8 ± 2.6	0.3 ± 0.1	2.44 ± 2.0	211 ± 41.9*	57.9 ± 36.2	1.22 ± 0.25	2.23 ± 1.17	0.7 ± 0.09	0.033 ± 0.002	0.95 ± 0.01
O_3 High	18.3 ± 3.1	16.5 ± 2.8*	1.8 ± 0.4*	1.78 ± 0.2*	232.4 ± 35.8*	88.7 ± 25.8	1.60 ± 0.15*	2.34 ± 0.26	0.8 ± 0.11	0.033 ± 0.002	0.93 ± 0.04
CB + O_3 Low	10.6 ± 3.4	10.5 ± 3.5	0.1 ± 0.1	1.57 ± 0.7	237 ± 93.9*	85.7 ± 14.4	1.73 ± 0.10*	2.28 ± 0.11	0.6 ± 0.03	0.037 ± 0.001	0.95 ± 0.03
CB + O_3 Med	15.4 ± 4.9	14.7 ± 4.5	0.7 ± 0.6	1.50 ± 1.0	268 ± 143*	51.3 ± 3	1.50 ± 0.15	2.43 ± 0.50	0.7 ± 0.06*	0.032 ± 0.002*	0.82 ± 0.05
CB + O_3 High	25.0 ± 1.4*#^$	22.0 ± 1.9*#^$	3.0 ± 0.7*#^$	3.80 ± 1.0*#^$	341.4 ± 42.6*#	207.1 ± 60.5*#^$	2.29 ± 0.19*#4.98 ± 0.55*#		0.8 ± 0.07*	0.030 ± 0.001*	0.85 ± 0 .06*

Bronchoalveolar lavage total cell, macrophages, neutrophils/pmn, LDH, total protein, and tissue hydrogen peroxide concentration after exposure to air (control), CB, O_3, and CB + O_3 at low (2.5 mg/m^3 and/or 0.5 ppm), medium (5.0 mg/m^3 and/or 1.0 ppm), and high (10.0 mg/m^3 and/or 2.0 ppm) 3 h, followed by euthanasia 24 h post-exposure. Data are presented as mean ± standard deviation. $n = 5$–8 mice per group. Data analyzed by 1-way ANOVA followed by Tukey's post hoc test.

* $p \leq .05$ versus control.

\# $p \leq .05$ CB + O_3 versus single exposure at same dose.

^ $p \leq .05$ CB + O_3 low versus high dose.

$ $p \leq .05$ CB + O_3 medium versus high dose.

while low concentration CB + O_3 and CB produced the lowest oxidant levels (Figure 2B). Figure 2C showing the ability of the particles to reduce antioxidant levels in human serum (FRAS assay) further confirmed similar oxidant production potential of the co-exposure particulate. The particulates were more potent at medium and high exposure levels while the low dose and CB ranked the lowest in potency.

Lung inflammation and injury

Lung inflammation was assessed by quantifying cellularity of the BAL fluid and by determining cell differentials. A dose dependence in total cell counts as well as macrophage and neutrophil counts was more evident in the case of co-exposure (Table 3). Co-exposure also demonstrated a greater induction in these indices compared with individual exposures. Both O_3 and CB + O_3 induced increased BAL total protein levels, however, the difference between O_3 and CB + O_3 were only statistically significant at the highest exposure levels (Table 3). Co-exposure significantly induced lung injury (LDH increase in BAL) at medium and high doses, while this response was only elicited by O_3 at the highest exposure levels (Table 3). The level of hydrogen peroxide (H_2O_2) in the lung tissue homogenate was significantly elevated by only the co-exposure at the highest tested dose (Table 3).

Lung histopathology was performed to assess the lung injury after exposure to low (2.5 mg/m^3 and 0.5 ppm O_3) and medium (5 mg/m^3 and 1 ppm) doses of CB, O_3, and CB + O_3. Control/air and CB exposed mice had no histopathological alterations though CB-laden macrophages were noted in CB exposed mice at both low and medium exposures (Figs. 3A, B, and E). Low dose O_3 alone exposure did not induce any inflammatory cell influx or bronchiolar epithelial necrosis, while medium dose O_3 did induce epithelial necrosis without associated cellular inflammation (Figs. 3C, F, and inset panel F). Co-exposure at both low and medium dose induced an influx of centriacinar inflammatory cells, mainly neutrophils, and airway epithelial necrosis (Figs. 3D, inset panel D, G, and inset panel G). Semiquantitative scoring for inflammation and epithelial necrosis is presented in Figures 3H and 3I. Macrophage hyperplasia was a feature of only co-exposure and was noted at both low and medium dose exposures (Figure 3J). Histopathological alterations after the high dose exposures were previously reported (Hathaway *et al.*, 2021; Majumder *et al.*, 2021a).

Benchmark dose response modeling was performed on the CB, O_3, and CB + O_3 dose response data using different lung injury and inflammatory responses measured. It is clear from this modeling that inflammation related parameters have lower BMD compared with injury parameters and a clear potentiation is seen with co-exposure (Table 4). We demonstrate that mixed inhalation exposure to CB and O_3 result in greater biological toxicity as indicated by a significant reduction in BMD. The reduction or increased toxicity observed was true as observed with the BMD calculated for all the pulmonary endpoints evaluated. In case of mixed exposure, CB dose reduces 2.24, 3.25, 21.81, and 12.58 fold for BALF LDH, proteins, total cell influx, and macrophage influx, respectively. Similarly, with O_3 the dose required for a BMD change reduces 2.84, 1.13, 2.30, and 1.36 fold for BALF LDH, proteins, total cell influx, and macrophage influx, respectively, for mixed exposures compared with O_3 alone. A lesser decrease in case of O_3 compared with greater magnitude changes in case of CB potentially indicate a greater contribution of O_3 in the observed responses. Principal component analysis (PCA) was performed to interpret the response from each animal from the multidimensional pulmonary injury and inflammation data. PCA of

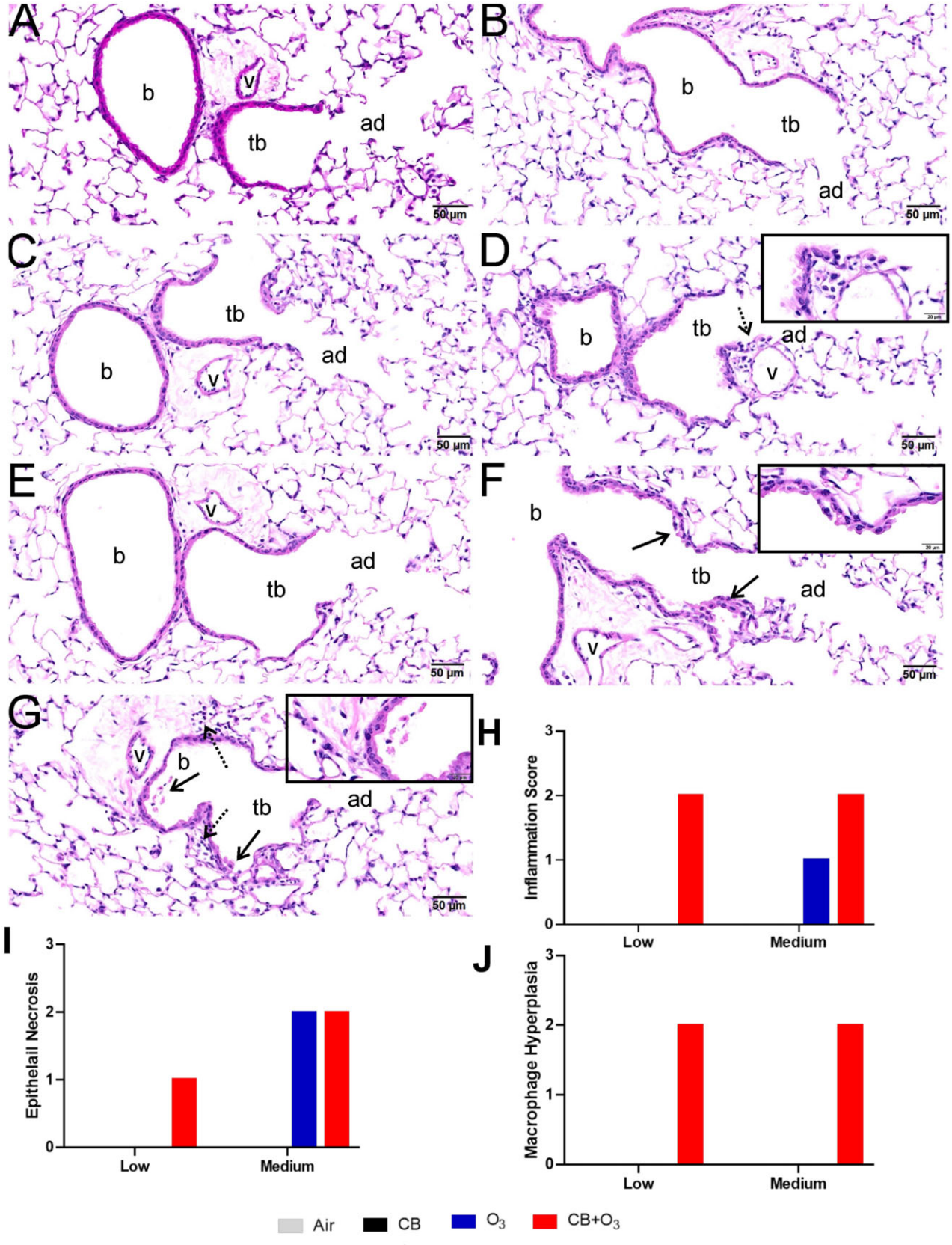

Figure 3. Histopathological assessments of lung tissue after low and medium dose exposures. Lung tissues were collected 24 h post-exposure, fixed in neutral buffered formalin, and stained with H&E. Light photomicrographs of sections from (A) filtered air, (B) CB 2.5 mg/m^3, (C) O_3 0.5 ppm, (D) CB + O_3 (2.5 mg/m^3 + 0.5 ppm), (E) CB 5.0 mg/m^3, (F) O_3 1.0 ppm, (G) CB +O_3 (5.0 mg/m^3 + 1.0 ppm). Tissues were semi-quantitatively scored in a blinded manner by a board-certified veterinary pathologist for (H) inflammatory cell influx, (I) airway epithelial injury/cell death, and (J) macrophage hyperplasia. b, bronchiole; tb, terminal bronchiole; ad, alveolar duct; v, blood vessel; stippled arrows, inflammatory cell infiltration; solid arrows, necrotic/exfoliated airway epithelial cells. Insets on (D), (F), and (G) are higher magnification on the areas where pathological lesions are noted.

Table 4. The BMD modeling of lung injury (BALF LDH and BALF total protein) and lung inflammation (total cell influx and alveolar macrophages) parameters after exposure to air (control), CB, O_3, and CB + O_3 for 3 h followed by euthanasia 24 h post-exposure

Exposure	BALF LDH		BALF Total Protein		Total Cell Influx		Alveolar Macrophages	
	BMD	BMDL	BMD	BMDL	BMD	BMDL	BMD	BMDL
CB (mg/m^3)	9.39	7.26	12.06	8.40	42.76	9.39	42.80	9.40
O_3 (ppm)	2.39	1.46	0.84	0.60	0.90	0.56	0.93	0.66
CB + O_3 (mg/m^3 + ppm)	4.19 + 0.84	3.5 + 0.71	3.7 + 0.74	2.7 + 0.55	1.96 + 0.39	1.43 + 0.29	3.4 + 0.68	2.9 + 0.58

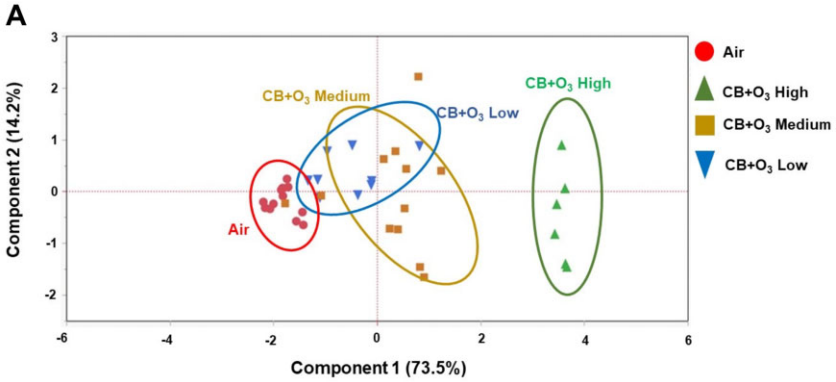

Figure 4. Score plot of the first 2 components of the principal component analysis showing pulmonary injury and inflammatory response after exposure to air (control), CB, O_3, and CB + O_3 at low (2.5 mg/m^3 and/or 0.5 ppm), medium (5 mg/m^3 and/or 1 ppm), and high (10 mg/m^3 and/or 2 ppm), for 3 h followed by euthanasia 24 h post-exposure. The response of animals from each group and their clustering was highlighted qualitatively by the oval.

the co-exposure groups clearly indicated a dose-dependent response (Figure 4). The response of low and medium concentrations clustered together and was closer to the response of air exposed animals. The high dose exposure, however, had a distinct response from the other 2 doses. The PCA loading plot further showed BALF LDH and total protein response was akin and the response from BALF PMN influx, BALF AM influx, and total cell influx was similar. PCA of all the exposures together presented in Supplementary Figure 1 shows similarity in response with animals exposed to high O_3 and medium dose of co-exposure, similarity in response of air with all doses of CB exposed animals, no change in response between low dose O_3 and low dose co-exposure, and a distinct response with high dose co-exposure.

Co-exposure induced lung function decline

Exposure to both medium (5 mg/m^3 +1 ppm) and high dose (10 mg/m^3 + 2 ppm) of CB + O_3 induced a significant increase in respiratory resistance (Rrs), a decrease in dynamic compliance (Crs), and decline in forced expiratory flow at 0.1 s (FEV0.1) in co-exposure animals compared with air (Table 3). However, no change in Rrs and FEV0.1 was observed in lower doses of co-exposure (2.5 mg/m^3 CB + 0.5 ppm O_3) or individual CB and O_3 exposures at any tested dose (Table 3).

Macrophage uptake of particles

CB uptake was quantified in lavage macrophage by (1) quantifying % of macrophages taking up particles and (2) by quantifying area occupied by CB in each macrophage (Figure 5A). A dose dependent increase in CB positive BAL macrophages number was observed, while in case CB + O_3 the number of cells was significantly lower than CB at medium and high doses (Figure 5B). Moreover, no dose-dependent increase was observed between medium and high doses. Further, we quantified area per macrophage occupied with CB aggregates and found a dose dependent increase with CB particles that was not observed in the case of CB + O_3 (Figure 5C).

Lung carbon burden after CB and CB + O_3 exposure

Lung burden was quantified 24 h post-exposure and after highest co-exposure (10 mg/m^3 CB + 2 ppm O_3). A significantly greater amount of CB (1.5 ± 0.05 μg/lung) was detected in the lungs of mice after co-exposure compared with the CB alone exposure (0.8 ± 0.08 μg/lung) (Figure 5D). At the medium dose co-exposure (5 mg/m^3 CB + 1 ppm O_3), we detected significant amount of CB in the lungs (1.1 ± 0.08 μg/lung) of co-exposure mice. However, the CB burden in the CB alone medium exposure was below the detection limit (0.8 μg CB) of our lung burden assay.

Correlation of aerosol characteristics with lung inflammation/injury parameters

Aerosol distribution (mobility/charge) and deposition correlations

Different aerosol physicochemical parameters can impact the biological outcome by changing deposition, uptake, and clearance. These relationships have been deciphered in detail for individual toxicants. However, the relative contribution of these parameters in mixed particulate and gas exposures have not been explored. In the current work, using correlation analysis we evaluated the strength of these associations between aerosol physicochemical characteristics and lung inflammation/injury. A comprehensive list of these correlations can be found in Supplementary Figure 2 and File 2. A heatmap based on the correlation coefficient values is presented as Figure 6A and top significant ($p \leq .05$) correlations are highlighted in Figure 6B. Charge-based aerosol size distribution was strongly and positively correlated with total and alveolar lung deposition ($r = 0.88$, CI [0.756–0.945]), BAL total cells ($r = 0.71$, CI [0.455–0.859]), and neutrophil counts ($r = 0.67$, CI [0.403–0.842]). Another top

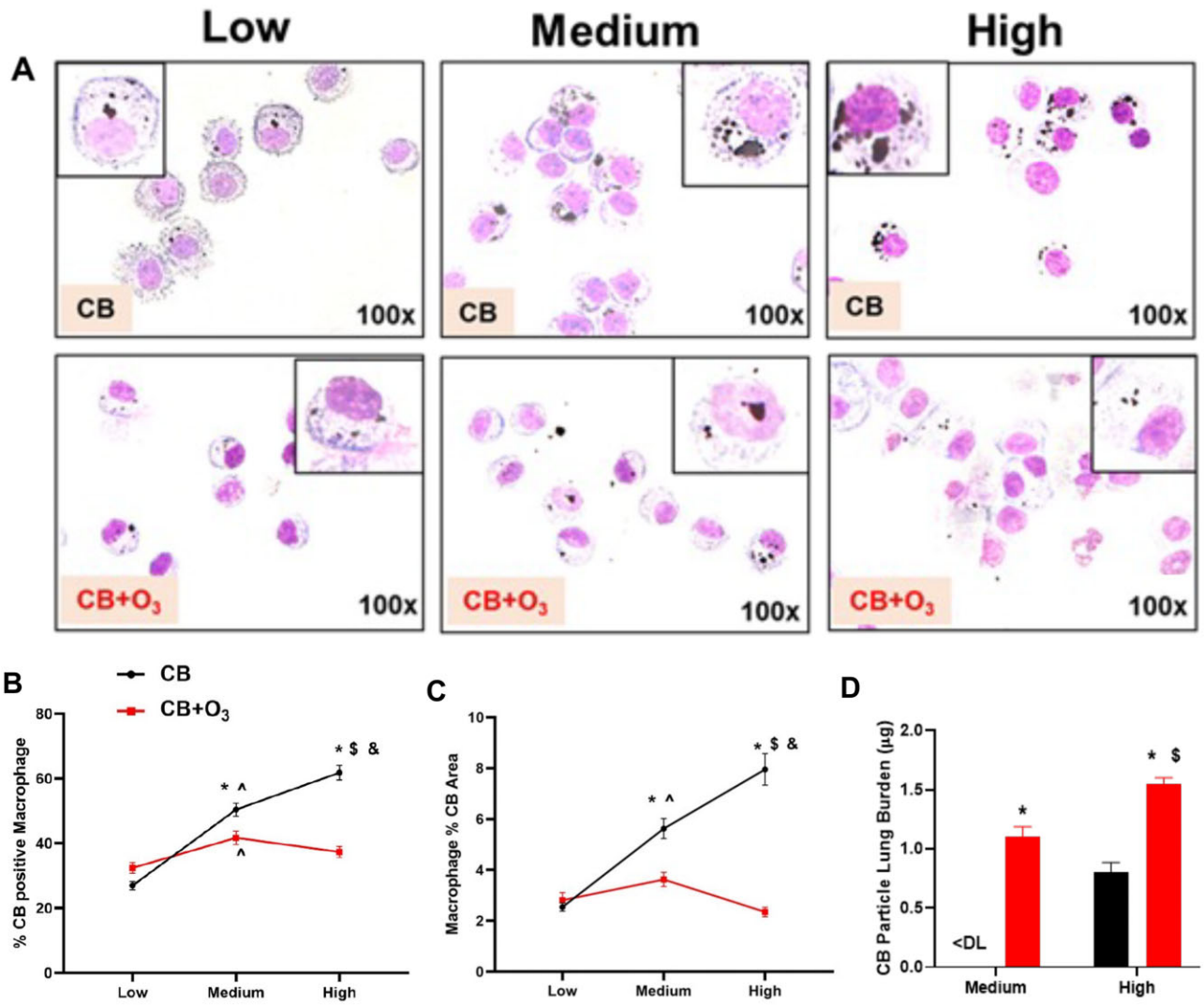

Figure 5. Particle uptake. A, Representative images of *in vivo* uptake of particles (CB and CB + O_3) by broncho-alveolar lavage macrophages (×40 and ×100 magnification) at low (0.5 ppm and/or 2.5 mg/m^3), medium (1 ppm and/or 5 mg/m^3), and high (2 ppm and/or 10 mg/m^3) exposures for 3 h, followed by euthanasia 24 h post-exposure. Quantification of particle uptake by (B) percentage particle positive macrophages and (C) percentage of particle area in macrophages. D, Lung burden quantification of particles (CB and CB + O_3) 24 h post-exposure. Data analyzed by 2-way ANOVA followed by Tukey's post hoc test. $^*p < .05$ versus CB + O_3 at same dose, $^\wedge p \leq .05$ low versus medium dose, $^\$p \leq .05$ medium versus high dose, $^\&p < .05$ low versus high dose. <DL denotes lower than detection limit of the assay (0.8 µg).

correlated parameter was total lung deposition that significantly positively correlated with BAL PMN/neutrophils ($r = 0.89$, CI [0.790–0.953]), BAL total cells ($r = 0.85$, CI [0.712–0.934]), BAL macrophages ($r = 0.75$, CI [0.530–0.883]), and BAL LDH ($r = 0.59$, CI [0.247–0.810]). Finally, alveolar deposition was significantly positively correlated with BAL PMN/neutrophils ($r = 0.89$, CI [0.789–0.953]), BAL total cells ($r = 0.85$, CI [0.712–0.934]), and BAL macrophages ($r = 0.75$, CI [0.530–0.883]). Similar patterns were obtained by spearman correlation (Supplementary Table 2). All these correlations were statistically significant ($p \leq .05$) and absolute significance is presented in Supplementary Table 2.

Aerosol oxidative potential correlations

When particulate have higher oxidation potential, the antioxidants levels in the human serum (used as a test substance) are at a lower level ($p \leq .05$) and it correlated with BAL total cells ($r = -0.90$, CI [0.958–0.778]), BAL macrophages ($r = -0.86$, CI [0.943–0.712]), and BAL PMN/neutrophils ($r = 0.86$, CI [0.943–0.712]). Spin probe CMH-based measurements by EPR demonstrated positive and significant ($p \leq .05$) correlation with BAL proteins ($r = 0.89$, CI [0.634–0.972]), BAL LDH ($r = 0.82$, CI [0.442–0.952]), and surface oxygen ($r = -0.98$, CI [0.998–0.938]). Particle surface oxygen measurement (XPS) demonstrated negative and significant ($p \leq .05$) correlation with BAL total cells ($r = -0.58$, CI [0.790–0.266]), BAL macrophages ($r = -0.57$, CI [0.738–0.248]), and BAL LDH ($r = -0.421$, CI [0.710–0.011]). Similar patterns were obtained by spearman correlation (Supplementary Figure 2 and Table 2). All these correlations were statistically significant ($p \leq .05$) and absolute significance is presented in Supplementary Table 2.

Lung tissue gene expression

Real time PCR-based gene expression at the mRNA level was performed on an array of genes. A manual annotation of groups of genes based on known functionality was performed (Figure 7A). In line with pulmonary injury and inflammation observed earlier, co-exposure induced gene expression changes were greater in magnitude compared with individual exposures and were more

A

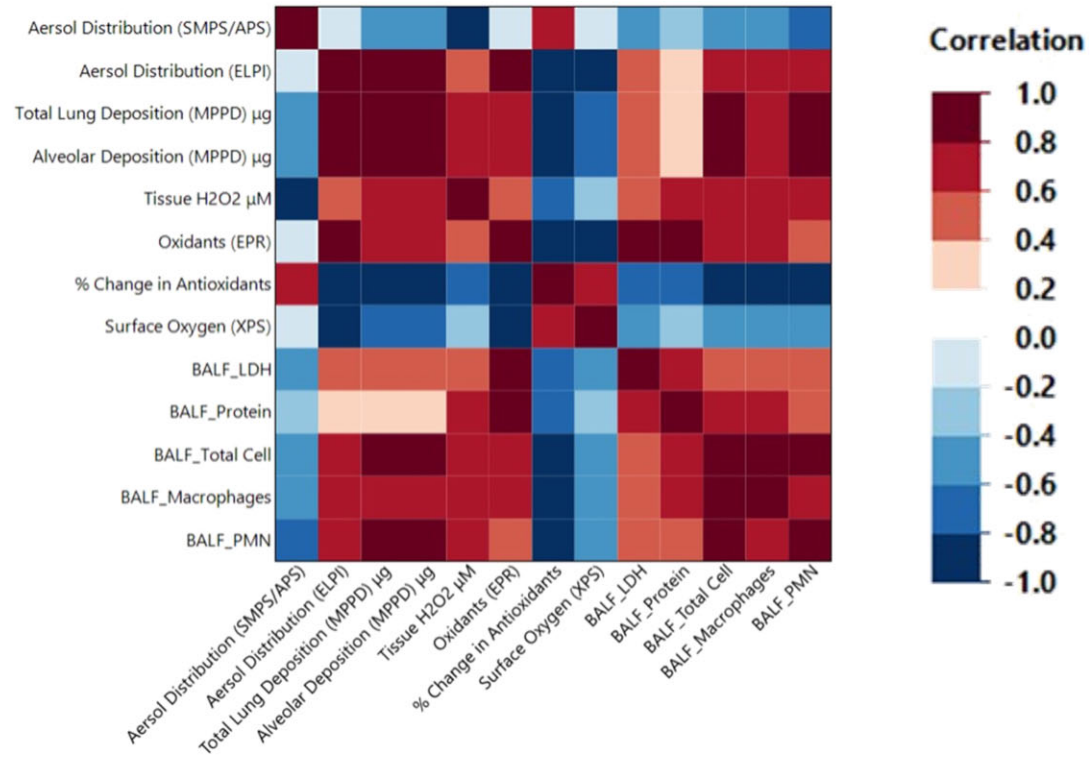

B

Characteristics		Top Correlated Variable	Pearson Correlations (Confidence Interval)
Aerosol Characteristics	**Aerosol Size Distribution (ELPI)**	Total and Alveolar Deposition	0.882 (0.756 – 0.945)
		BALF Total Cells	0.712 (0.455 – 0.859)
		BALF PMN	0.679 (0.403 – 0.842)
	Total Lung Deposition (MPPD)	BALF PMN	0.899 (0.790 – 0.953)
		BALF Total Cells	0.859 (0.712 – 0.934)
		BALF Macrophages	0.757 (0.530 – 0.883)
		BALF LDH	0.598 (0.247 – 0.810)
	Alveolar Deposition (MPPD)	BALF PMN	0.899 (0.789 – 0.953)
		BALF Total Cells	0.859 (0.712 – 0.934)
		BALF Macrophages	0.757 (0.530 – 0.883)
Oxidative Characteristics	**% Change in Antioxidants (FRAS)**	BALF Total Cells	-0.901 (-0.958 – -0.778)
		BALF Macrophage	-0.869 (-0.943 – -0.712)
		BALF PMN	-0.869 (-0.943 – -0.712)
	Oxidants (EPR)	BALF Protein	0.893 (0.634 – 0.972)
		BALF LDH	0.823 (0.442 – 0.952)
		Surface Oxygen	-0.989 (-0.998 – -0.938)
	Surface Oxygen (XPS)	BALF Total Cell	-0.587 (-0.790 – -0.266)
		BALF Macrophages	-0.574 (-0.738 – -0.248)
		BALF LDH	-0.421 (-0.710 – -0.011)

Figure 6. Multivariate analysis linking aerosol characteristics and oxidative properties of the mixtures to pulmonary injury and inflammation. A) Heat map representing Pearson correlations of aerosol characteristics and oxidative characteristics of the mixtures with biological outcomes. B) Table outlining the top correlated biological variables with aerosol characteristics and oxidative characteristics based on *p*-value.

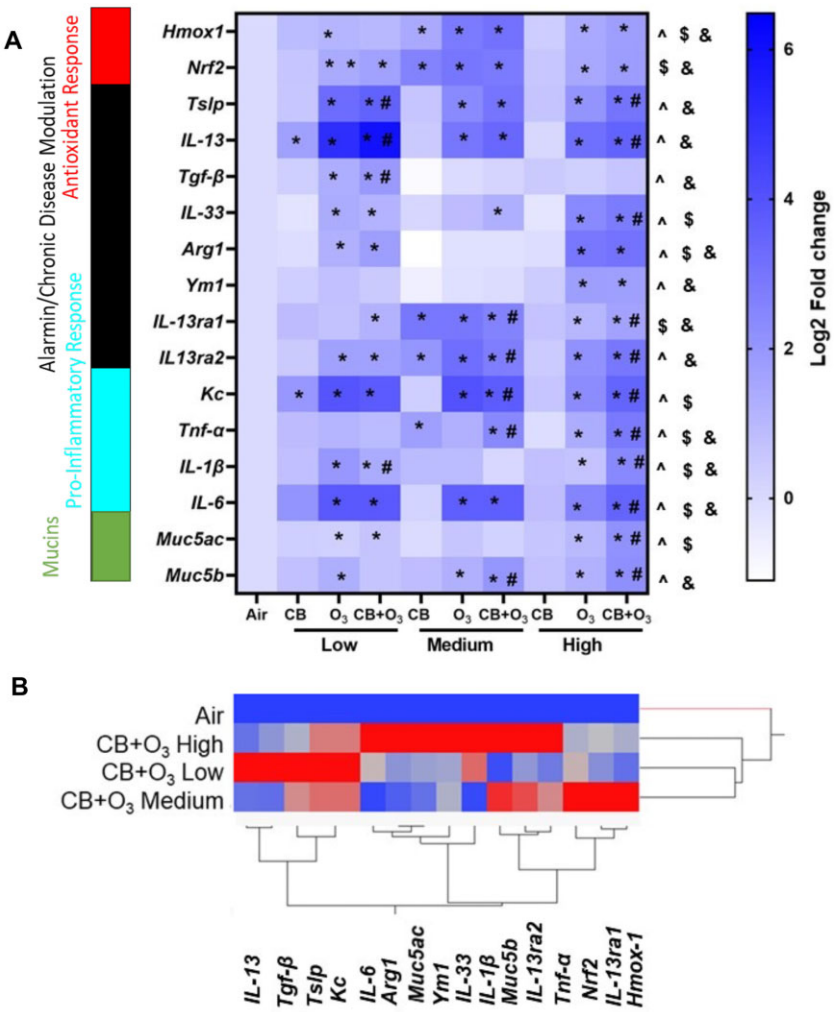

Figure 7. Lung tissue real-time mRNA expression. A) Heat Map representing the fold changes of mRNA gene expression in lung tissue after exposure to air (control), CB, O_3, and CB + O_3 at low (2.5 mg/m^3 and/or 0.5 ppm), medium (5.0 mg/m^3 and/or 1 ppm), and high (10.0 mg/m^3 and/or 2.0 ppm), for 3 h, followed by euthanasia 24 h post-exposure. The values are normalized to Log2-fold change. Data analyzed by 2-way ANOVA followed by Tukey's post hoc test. *$p < .05$ versus control, #$p \leq .05$ versus CB + O_3 single exposure at same dose, ^$p \leq .05$ CB + O_3 low versus high dose, \$$p \leq .05$ CB + O_3 medium versus high dose, &$p \leq .05$ CB + O_3 low versus medium dose. B) Hierarchical clustering analysis (HCA) of mRNA gene expression after exposure to air (control) and CB + O_3 at low (2.5 mg/m^3 + 0.5 ppm), medium (5.0 mg/m^3 + 1.0 ppm), and high (10.0 mg/m^3 + 2.0 ppm) doses, for 3 h, followed by euthanasia 24 h post-exposure.

prominent at either lower or higher end of the exposure spectrum. This response was significant ($p \leq .05$) except in case of antioxidant genes which show similar induction by both high dose O_3 and CB + O_3. Genes related to alarmin signaling/chronic disease modulation (*Tslp, Il-33, Il-13, Il-13ra1, Il13ra2*), pro-inflammatory response (*Kc, Tnf-α, Il-1β, IL-6*) and mucin (*Muc5ac, Muc5b*) also demonstrated similar pattern. M2 macrophage polarization markers (*Arg1, Ym1*), usually induced in chronic diseases, were increased at the lowest and highest dose but not at the medium dose, while *Tgf-β* was only induced at the lowest dose. Antioxidant response genes (nuclear factor-erythroid factor 2-related factor 2 (*Nrf2*) and *Hmox-1*) were induced maximally at the medium exposure levels for both O_3 and CB + O_3. Interestingly, *IL-13, Tgf-β*, and *Tslp* demonstrated more significant mRNA expression induction at the lowest exposure than higher exposures. An HCA approach was also performed for the co-exposure groups to evaluate the grouping of genes based on exposure dose (Figure 7B). This approach yielded different grouping of genes compared with the literature-based functional annotation that is presented in Figure 6A. This approach yielded groups of genes that responded maximally to the lowest dose (*Il-13, Tgf-β, Tslp*, and *Kc*), medium dose (*Muc5b, Il-13ra2, Nrf2, Il-13ra1, Hmox-1*) and the highest dose (*Arg1, Muc5ac, Ym1, Il-33, Il-1β, Muc5b, Il-13ra2, Tnf-α*).

BALF inflammatory mediator secretion and predictor screening

An array of mediators were quantified using ELISA on BAL fluid. Secretion of all the mediators (IL-13, IL-6, TSLP, KC, IL-1β, transforming growth factor beta [TGF-β], and TNF-α) was significantly ($p \leq .05$) increased by the co-exposure at the highest tested dose (Figure 8A). Secreted cytokines can be grouped based on distinct patterns of secretion. The first group, which showed enhanced secretion without a clear dose response pattern, consisted of dual function (pro- and anti-inflammatory) cytokines (IL-6, IL-13) and epithelial alarmin TSLP. Interestingly, the greatest increase in IL-13 levels were noted after co-exposure at all the tested co-exposure concentrations. A significant increase (compared with control) in the secretion of IL-6 and IL-13 was also noted by O_3 exposure at the highest exposure level. The second group

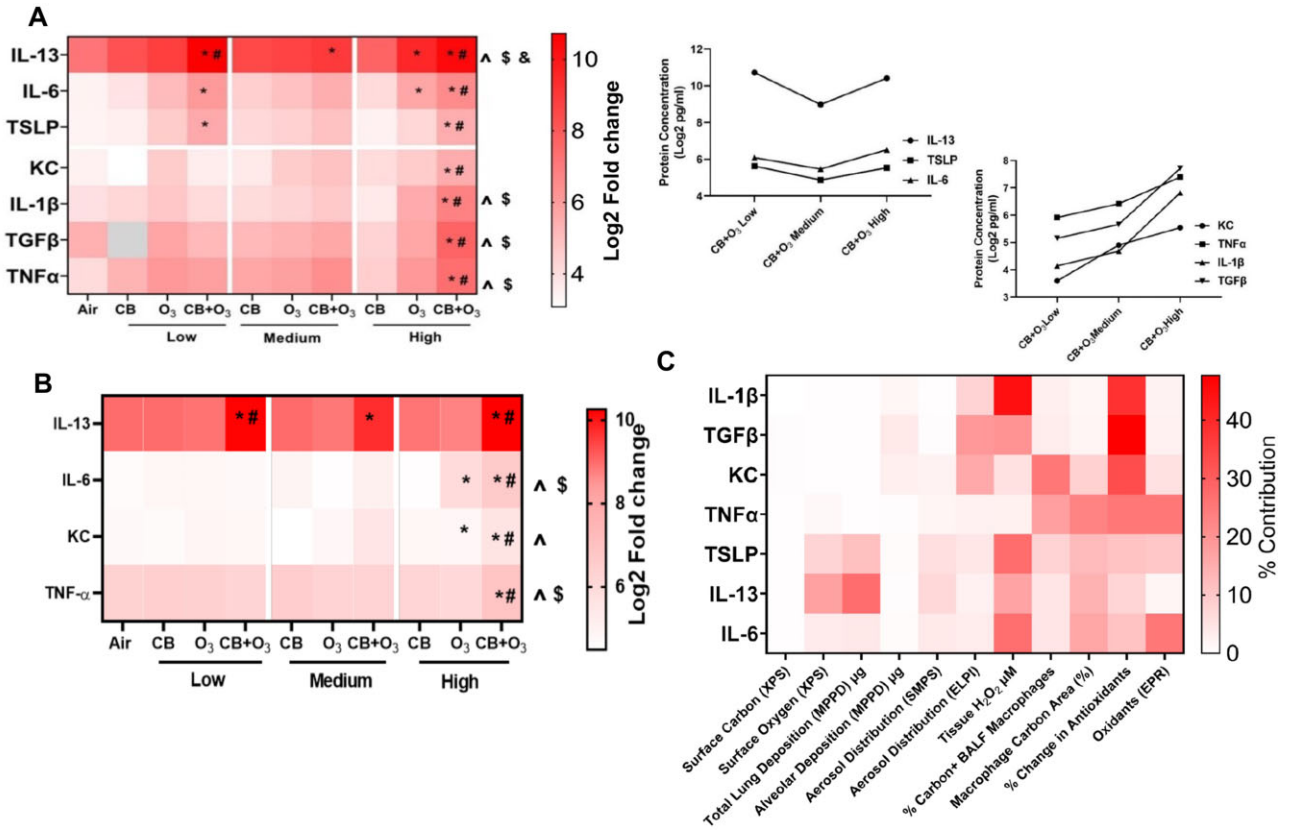

Figure 8. Predictor screening of broncho-alveolar lavage cytokines. A) Heat map representing the cytokine quantification in broncho-alveolar lavage fluid after exposure to air (control), CB, O_3, and CB + O_3 at low (2.5 mg/m^3 and/or 0.5 ppm), medium (5.0 mg/m^3 and/or 1.0 ppm), and high (10.0 mg/m^3 and/or 2.0 ppm) doses for 3 h followed by euthanasia 24 h post-exposure. B) Heat map representing the cytokine quantification in lung tissue homogenate after exposure to air (control), CB, O_3, and CB + O_3 at low (2.5 mg/m^3 and/or 0.5 ppm), medium (5.0 mg/m^3 and/or 1.0 ppm), and high (10.0 mg/m^3 and/or 2.0 ppm) doses for 3 h followed by euthanasia 24 h post-exposure The values are normalized to Log2 fold change. Data analyzed by 2-way ANOVA followed by Tukey's post hoc test. *$p < .05$ versus control, #$p \leq .05$ CB + O_3 versus single exposure at same dose, ^$p \leq .05$ CB + O_3 low versus high dose, \$$p \leq .05$ CB + O_3 medium versus high dose, &$p \leq .05$ CB + O_3 low versus medium dose. C) Heat map representing percentage contribution of aerosol characteristics in cytokine production based on boot strap forest approach.

consisted of typical inflammatory cytokines such as KC, TNF-α, IL-1B, and chronic disease modulator TGF-β. These cytokines followed a dose-response dependent increase.

Lung tissue homogenate were evaluated for the cytokine/chemokine (IL-13, IL-6, KC, and TNF-α) levels (Figure 8B). A significant increase in all these cytokine/chemokines were seen after highest dose co-exposure (10 mg/m^3 CB + 2 ppm O_3). IL-13 was induced by co-exposure at all the exposure levels, whereas IL-6 was also induced by O_3 at 2 ppm. This demonstrated a similar trend as lavage ELISA.

A boot strap forest-based machine learning approach was utilized to study the relative contribution of different aerosol characteristics in cytokine production (Figure 8C). Oxidative status (antioxidant depletion capacity of the aerosol and lung tissue H_2O_2 levels) was among the significant contributors for IL-1β, KC, and TGF-β secretion, whereas uptake was most significant contributor for the rest of the cytokines.

Discussion

In this study, we aimed at understanding the pulmonary toxicity of ultrafine CB and O_3 inhalation co-exposure at different exposure levels and attempted to determine the correlation/contribution of different physiochemical characteristics in lung injury and inflammation. We demonstrated that co-exposure causes significantly greater pulmonary toxic potential compared with individual exposures as evidenced by sharp decrease in BMD. Quantifying the uptake of the mixtures and evaluating the toxicity showed interesting relationship between uptake and toxicity for mixtures. In addition, using multivariate analysis we elaborate the correlation of physicochemical and oxidative characteristics of the mixtures to pulmonary injury and inflammation. A boot strap forest approach predicted relative contribution of different physiochemical characteristics on the response of individual cytokines measured.

We previously described mechanisms of lung inflammation and lung function decline after inhalation co-exposure to CB and O_3 (Majumder *et al.*, 2021a). The highest particle dose in that study was equivalent to an alveolar deposited dose of a worker after 8 h exposure at the current U. S. Occupational Safety and Health Administration (OSHA) permissible exposure limit (3.5 mg/m^3) (Majumder *et al.*, 2021a). This dose translated to 35 days of PM 2.5 exposures at current national ambient air quality standard (35 µg/m^3). In addition, a 2-ppm dose was selected for exposure to O_3 alone that is 4 times the dose capable of inducing neutrophilia in humans. This selection was made keeping in consideration differences in deposition due to differences in human and murine anatomy (Hatch *et al.*, 1994, 2013). However, here we report additional findings to considerably lower concentrations of both CB (equivalent exposure of 17.5 and 8.75 days of PM 2.5 exposure at current permissible concentrations) and O_3 exposures at 2 times and same dose

that induces neutrophilia. Thus, utilizing more relevant exposure concentrations, we are providing a detailed evaluation of co-exposure responsive lung inflammatory and injury markers as well as describe the correlations of different aerosol characteristics with lung toxicity.

Our findings of increased CB retention in the lung in case of CB and O_3 co-exposure indicate the possibility of persistent adverse outcomes as retention of particulates in the lungs has been linked to chronic pulmonary phenotypes in case of a variety of environmental exposures and engineered nanoparticle exposures (Fraser *et al.*, 2021; Oberdorster *et al.*, 1994, 2015; Riediker *et al.*, 2019). Furthermore, as this co-exposure particles can produce more reactive oxygen species (detected in the lungs and systemic circulation) this increase the possibility of aggravating systemic diseases and for an extended period. Lung function data confirm the changes in functional respiratory parameters (Rrs, Crs, and FEV0.1) after exposure to medium and high co-exposure concentrations, whereas individual exposures and low dose co-exposure did not induce any functional change. These observations at the highest dose exposures are in line with our recently published study using a similar dose (Majumder *et al.*, 2021a). This data clearly point toward a greater functional impact of co-exposure compared with individual exposures at medium and high doses.

The dose response data were used to determine relative potency of the test aerosols using BMD modeling. The BMD approach is statistically more robust and resulting values are inherently less uncertain than other dose response metrics. This approach has been used to understand responses of other inhaled particulate pollutants (engineered nanomaterials and fibers) (Kuempel *et al.*, 2006; O'Brien and Cummins 2010; Pink *et al.*, 2020; Weldon *et al.*, 2018). Here, we describe a significant reduction in both CB and O_3 dose in the case of mixed exposures which confirms our previous findings of increased biological activity of mixed CB and O_3 exposure compared with single toxicant exposures (Hathaway *et al.*, 2021; Majumder *et al.*, 2021a).

Uptake of particulate materials (particulate matter, engineered nanoparticles) in most of the cases is considered essential for biological activity (Hussain *et al.*, 2009; Maynard *et al.*, 2006; Patel *et al.*, 2015; Zheng *et al.*, 2018). We previously demonstrated that after O_3-reacted CB particle exposure, macrophages released CXCR3 receptor ligands that play an important role in the endothelial cell responses (impaired scratch healing and monolayer permeability) (Majumder *et al.*, 2021b). Here, in case of CB exposure alone, we observed a linear increase in % macrophages in lavage that take up the particulate. However, in the case of co-exposure this response plateaued with medium and high dose. At these 2 doses there was not a significant increase in % macrophages that take up the particulates. When compared with CB, in the CB + O_3 group, a significantly smaller number of macrophages were detected to contain CB aggregates at medium and high exposure levels. The increase in toxicity and plateau of uptake suggests increased biological potency and a differential surface reactivity of the co-exposure aerosols. Although we observe that similar characteristics are involved in single and co-exposure outcomes, it is important to note that the potency is significantly enhanced. Surface reactivity can be deduced from the acellular assays such as oxidant generation capacity (EPR study using spin probe CMH) and reduction of antioxidants in human serum (FRAS assay). These findings further corroborate the conclusion that interaction with O_3 increased surface reactivity of CB particles. However, it is important to note that while both medium and high exposures produced similar oxidant levels by EPR analysis, FRAS assay indicated a dose-dependent antioxidant depletion. Multiple published reports confirm the utility of FRAS assay in detecting the oxidative potential of the particulate materials (Fraser *et al.*, 2020; Rogers *et al.*, 2008). Moreover, it is important to note that we recently demonstrated that reactive oxygen species generation is a critical factor behind enhanced biological activity of the co-exposure (Hathaway *et al.*, 2021; Majumder *et al.*, 2021a,b). Thus, in case of mixed exposures, while we are seeing similar physicochemical characteristics involved in toxic response, oxidant dependence is significantly greater.

Increasing concentration of mixed exposure leads to a decrease in the CB aggregate area in macrophages, while a dose dependent increase was observed in the case of CB alone. A potential explanation of this change is increased toxicity leading to macrophage cell death. Indeed, we observed increased LDH release with increasing co-exposure doses. Previous literature confirms increased toxicity of macrophages after exposure to varied air pollutants including PM, O_3, and ultrafine/nanoparticles (Devlin *et al.*, 1994; Gowdy *et al.*, 2021; Patial and Saini 2020; Sunil *et al.*, 2012; Wei *et al.*, 2021; Wottrich *et al.*, 2004). However, the increase in LDH could be due to toxicity of several cell types including epithelial cells and non-mono-nuclear cells (neutrophils, etc.). A potential reduction in phagocytic ability due to the co-exposure can also result in similar result. Particulate exposures are known to impact the uptake mechanisms which can result in altered bacteria/virus uptake (Hussain *et al.*, 2009; Pacheco *et al.*, 2013; Vranic *et al.*, 2013). This can have serious consequences in terms of clearance of a later infection and mounting an effective immune response. Work is currently being performed to further elaborate on these mechanisms. However, as demonstrated by us previously and in this manuscript, there is an increased ROS production in the lungs. Oxidant generation can lead to reduced phagocytic ability (Anderson *et al.*, 2002) and cell death (Hussain *et al.*, 2010). We previously demonstrated that uptake of CB particles in the epithelial cells occur by both energy dependent and independent processes and recently reported a decrease in ATP production after CB and O_3 co-exposure (Hathaway *et al.*, 2021). A consequence of these processes is an increased lung burden of CB in case of O_3 (co-exposure scenario). Alternatively, the reduction in uptake at higher doses can potentially be a homeostatic/protective mechanism induced due to alterations in the cellular metabolic state (Caceres *et al.*, 2020). The Ym1 and Arginase 1 (Arg1) are M2 phenotype markers and M2 macrophages have been shown to express higher phagocytosis abilities (Schulz *et al.*, 2019). This potentially indicates a homeostatic response to clear the particles. The impacts on macrophage death/survival and endocytosis abilities can happen together or independent of each other. Further studies are ongoing to elaborate the mechanisms involved in these processes.

Apart from pulmonary injury and inflammation, we showed significant alteration in mRNA and protein secretions with co-exposures compared to single exposures. An enhanced biological activity of co-exposure compared with individual exposures was evident even at the lowest dose for *Tslp*, *Il-13*, *Tgf-β*, and *Il-1β*. These genes are known to play an important role in chronic pulmonary disorders such as asthma, chronic obstructive pulmonary disease (COPD), and fibrosis (Kabesch *et al.*, 2006; Verma *et al.*, 2018; Wang *et al.*, 2018). In general, co-exposure induced gene expression changes were more prominent at either the lower or higher end of the exposure spectrum. Antioxidant response genes (*Hmox-1* and *Nrf-2*) did not follow the pattern of the earlier genes. *Nrf-2* is a master regulator of cellular antioxidant defenses and is

known to play an important role in O_3 induced pulmonary damage (Cervellati *et al.*, 2020; Cho *et al.*, 2013; Henriquez *et al.*, 2017). *Hmox-1* is an antioxidant enzyme induced by a multitude of oxidative stimuli and is also implicated in O_3 induced (Li *et al.*, 2000; Takahashi *et al.*, 1997). The antioxidant response genes did not induce greater gene expression compared with individual exposures. This could be due to an impaired capacity of the lungs to mount an antioxidant response after co-exposures. Taken together, we saw an increased antioxidant depletion capacity and greater H_2O_2 production with co-exposures, translating into a more serious oxidative imbalance. Oxidative imbalances play a significant role in air pollution induced toxicity as well as in the pathogenesis of multiple chronic disorders that are exacerbated by air pollution (Ambroz *et al.*, 2016; Domej *et al.*, 2014; Kelly and Fussell, 2017). Lung has a complex architecture including multiple cell types and a myriad of other components that can influence redox balance including glutathione, lipids, and surfactants. In the current work, we have evaluated the pulmonary damage, inflammation, and uptake using recovered BALF and a broader pathological understanding is needed to fully understand the alterations occurring at the organ level. Although macrophages are the primary responders involved in particle clearance and as such the uptake was evaluated in recovered alveolar macrophages from BALF, more work is warranted to understand the uptake by other cell types and evaluate spatial interactions with various redox elements present in the lung.

Our results collectively point toward a chronic disease conducive phenotype, *ie*, over expression of M2 macrophage markers (Arg1 and Ym1), mucin genes (*Muc5b* and *Muc5c*) and IL-13 secretion. These findings corroborate the findings of increased IL-13 levels after air pollution exposure and their potential role in chronic disease susceptibility (Nadeau *et al.*, 2010; Pourazar *et al.*, 2004; Williams *et al.*, 2008). In addition, these results have a mechanistic aspect as IL-13 is known inducer of mucin genes, M2 macrophage phenotype, and Th2 dominated immune response in chronic respiratory diseases such as asthma and COPD (de Vries, 1998; Duffield, 2003; McKenzie *et al.*, 1993).

Our study has multiple strengths including a realistic co-exposure system, use of multiple doses of O_3 and CB ranging from occupational to environmental exposure scenarios providing relevant deposition levels, use of statistical approaches to identify the correlation of biological outcomes with aerosol physicochemical characteristics, use of a BMD approach for ranking of exposures, and evaluation of multiple readouts for inflammation and injury. However, our study does have some limitations that include use of male mice only, use of fixed ratio for CB and O_3, and use of single exposure at relatively higher exposure concentration rather than a chronic exposure scenario. We observed a discordance between the mRNA expression and protein expression levels. Genome wide research conducted over the last 2 decades showed although correlation exists between mRNA and protein expression levels, such patterns are far from perfect. This could be due to various factors including transcription to translational defects, post-translational modifications, cyclic expression with check points and due to timing lag between mRNA and protein expression. Further expansive temporal studies are required to decipher these interesting trends and such studies will hopefully elaborate the differentially observed effects.

In conclusion, the BMD of the pulmonary injury and inflammation response demonstrates that inhalation co-exposure to CB and O_3 result in greater pulmonary toxicity compared with individual CB or O_3 exposures. Interestingly, the uptake of the particulate was suppressed with an increasing dose of the CB + O_3 mixture, but the toxicity escalated with increasing dose of the mixture, suggesting that the particles from CB + O_3 mixtures at higher dose were more potent in inducing toxicity. We also identified aerosol physicochemical characteristics of the mixtures that correlated with biological outcomes and predict the relative contribution of these parameters on individual inflammatory cytokine secretions. Our results indicate a greater modulation of chronic disease mediators by the co-exposure at the lowest tested levels that points towards a greater potential to exacerbate chronic pulmonary disease. Further research is underway with even more reduced levels of both CB and O_3 as well as using animal models of respiratory disorders to further investigate the pathophysiological impacts of co-exposure. With this study and our recent work, we have detailed the interactive outcomes after ultrafine CB and O_3 inhalation exposure. Future studies should investigate the impact of different mixing ratio of O_3 and CB and chronic exposure at ambient levels to further elucidate the interactive outcomes in this exposure model.

Supplementary data

Supplementary data are available at *Toxicological Sciences* online.

Acknowledgments

Authors are grateful for excellent help by Dr James Wagner (MSU) for histopathology and for technical assistance by Kevin Engels, Zirong (Sherry) Xie, Tom Batchelor, and Qiang Wang.

Funding

National Institute of Environmental Health Sciences (R01 ES031253 to S.H.), National Institute of General Medical Sciences (U54GM104942 to S.H.), National Institute of Environmental Health Sciences (R01 ES015022 to T.R.N.), National Institute of Diabetes and Digestive and Kidney Diseases (R01 DK124510 to E.E.K.), P20 GM109098 (E.E.K.), National Institute of Aging (R56 NS117754 to E.E.K.), National Institute for Occupational Safety and Health (NTRC # 9390BN6 to V.K.), and National Heart, Lung, and Blood Institute (HL153532 to E.E.K.).

Declaration of conflicting interests

The authors declared no potential conflicts of interest with respect to the research, authorship, and/or publication of this article.

References

Ambroz, A., Vlkova, V., Rossner, P., Jr., Rossnerova, A., Svecova, V., Milcova, A., Pulkrabova, J., Hajslova, J., Veleminsky, M., Jr., Solansky, I., *et al.* (2016). Impact of air pollution on oxidative DNA damage and lipid peroxidation in mothers and their newborns. *Int. J. Hyg. Environ. Health* **219**, 545–556.

Anderson, H. A., Englert, R., Gursel, I., and Shacter, E. (2002). Oxidative stress inhibits the phagocytosis of apoptotic cells that have externalized phosphatidylserine. *Cell Death Differ.* **9**, 616–625.

Anenberg, S. C., West, J. J., Yu, H. B., Chin, M., Schulz, M., Bergmann, D., Bey, I., Bian, H. S., Diehl, T., Fiore, A., *et al.* (2014). Impacts of

intercontinental transport of anthropogenic fine particulate matter on human mortality. *Air Qual. Atmos. Health* **7**, 369–379.

Apte, J. S., Marshall, J. D., Cohen, A. J., and Brauer, M. (2015). Addressing global mortality from ambient PM2.5. *Environ. Sci. Technol.* **49**, 8057–8066.

Birnbaum, H. G., Carley, C. D., Desai, U., Ou, S., and Zuckerman, P. R. (2020). Measuring the impact of air pollution on health care costs. *Health Aff. (Millwood)* **39**, 2113–2119.

Braakhuis, H. M., Park, M. V., Gosens, I., De Jong, W. H., and Cassee, F. R. (2014). Physicochemical characteristics of nanomaterials that affect pulmonary inflammation. *Part. Fibre Toxicol.* **11**, 18.

Caceres, L., Paz, M. L., Garces, M., Calabro, V., Magnani, N. D., Martinefski, M., Adami, P. V. M., Caltana, L., Tasat, D., Morelli, L., *et al.* (2020). Nadph oxidase and mitochondria are relevant sources of superoxide anion in the oxinflammatory response of macrophages exposed to airborne particulate matter. *Ecotox. Environ. Safe* **205**, 111186.

Campen, M. J., Buntz, J., Lund, A., Seagrave, J., Vedal, S., Mauderly, J., and McDonald, J. (2009). Vascular effects of vapor and particulate phases of traffic-related air pollution: Initial results from the NPACT initiative. *Am. J. Resp. Crit. Care* **179**, A3150.

Cervellati, F., Woodby, B., Benedusi, M., Ferrara, F., Guiotto, A., and Valacchi, G. (2020). Evaluation of oxidative damage and Nrf2 activation by combined pollution exposure in lung epithelial cells. *Environ. Sci. Pollut. Res. Int.* **27**, 31841–31853.

Cho, H. Y., Gladwell, W., Yamamoto, M., and Kleeberger, S. R. (2013). Exacerbated airway toxicity of environmental oxidant ozone in mice deficient in Nrf2. *Oxid. Med. Cell. Longev.* **2013**, 254069.

Cleary, E. G., Cifuentes, M., Grinstein, G., Brugge, D., and Shea, T. B. (2018). Association of low-level ozone with cognitive decline in older adults. *J. Alzheimers. Dis.* **61**, 67–78.

de Vries, J. E. (1998). The role of IL-13 and its receptor in allergy and inflammatory responses. *J. Allergy Clin. Immunol.* **102**, 165–169.

Devlin, R. B., McKinnon, K. P., Noah, T., Becker, S., and Koren, H. S. (1994). Ozone-induced release of cytokines and fibronectin by alveolar macrophages and airway epithelial cells. *Am. J. Physiol.* **266**, L612–619.

Domej, W., Oettl, K., and Renner, W. (2014). Oxidative stress and free radicals in COPD–implications and relevance for treatment. *Int. J. Chron. Obstruct. Pulmon. Dis.* **9**, 1207–1224.

Duffield, J. S. (2003). The inflammatory macrophage: A story of Jekyll and Hyde. *Clin. Sci. (Lond.)* **104**, 27–38.

Elder, A., Gelein, R., Finkelstein, J. N., Driscoll, K. E., Harkema, J., and Oberdorster, G. (2005). Effects of subchronically inhaled carbon black in three species. I. Retention kinetics, lung inflammation, and histopathology. *Toxicol. Sci.* **88**, 614–629.

Farhat, S. C. L., Almeida, M. B., Silva-Filho, L., Farhat, J., Rodrigues, J. C., and Braga, A. L. F. (2013). Ozone is associated with an increased risk of respiratory exacerbations in patients with cystic fibrosis. *Chest* **144**, 1186–1192.

Fauroux, B., Sampil, M., Quenel, P., and Lemoullec, Y. (2000). Ozone: A trigger for hospital pediatric asthma emergency room visits. *Pediatr. Pulmonol.* **30**, 41–46.

Filipsson, A. F., Sand, S., Nilsson, J., and Victorin, K. (2003). The benchmark dose method–review of available models, and recommendations for application in health risk assessment. *Crit. Rev. Toxicol.* **33**, 505–542.

Franca, A., Aggarwal, P., Barsov, E. V., Kozlov, S. V., Dobrovolskaia, M. A., and Gonzalez-Fernandez, A. (2011). Macrophage scavenger receptor a mediates the uptake of gold colloids by macrophages in vitro. *Nanomedicine (Lond.)* **6**, 1175–1188.

Fraser, K., Hubbs, A., Yanamala, N., Mercer, R. R., Stueckle, T. A., Jensen, J., Eye, T., Battelli, L., Clingerman, S., Fluharty, K., *et al.* (2021). Histopathology of the broad class of carbon nanotubes and nanofibers used or produced in U.S. Facilities in a murine model. *Part. Fibre Toxicol.* **18**, 47.

Fraser, K., Kodali, V., Yanamala, N., Birch, M. E., Cena, L., Casuccio, G., Bunker, K., Lersch, T. L., Evans, D. E., Stefaniak, A., *et al.* (2020). Physicochemical characterization and genotoxicity of the broad class of carbon nanotubes and nanofibers used or produced in U.S. Facilities. *Part. Fibre Toxicol.* **17**, 62.

GBD 2015 Chronic Respiratory Disease Collaborators. (2017). Global, regional, and national deaths, prevalence, disability-adjusted life years, and years lived with disability for chronic obstructive pulmonary disease and asthma, 1990-2015: A systematic analysis for the global burden of disease study 2015. *Lancet Respir. Med.* **5**, 691–706.

GBD 2015 Risk Factors Collaborators. (2016). Global, regional, and national comparative risk assessment of 79 behavioural, environmental and occupational, and metabolic risks or clusters of risks, 1990-2015: A systematic analysis for the global burden of disease study 2015. *Lancet* **388**, 1659–1724.

Ghosh, R., Causey, K., Burkart, K., Wozniak, S., Cohen, A., and Brauer, M. (2021). Ambient and household pm2.5 pollution and adverse perinatal outcomes: A meta-regression and analysis of attributable global burden for 204 countries and territories. *PLoS Med.* **18**, e1003718.

Gowdy, K. M., Kilburg-Basnyat, B., Hodge, M. X., Reece, S. W., Yermalitsk, V., Davies, S. S., Manke, J., Armstrong, M. L., Reisdorph, N., Tighe, R. M., *et al.* (2021). Novel mechanisms of ozone-induced pulmonary inflammation and resolution, and the potential protective role of scavenger receptor bi. *Res. Rep. Health Eff. Inst.* (204), 1–49.

Haber, L. T., Dourson, M. L., Allen, B. C., Hertzberg, R. C., Parker, A., Vincent, M. J., Maier, A., and Boobis, A. R. (2018). Benchmark dose (BMD) modeling: Current practice, issues, and challenges. *Crit. Rev. Toxicol.* **48**, 387–415.

Hamade, A. K., Misra, V., Rabold, R., and Tankersley, C. G. (2010). Age-related changes in cardiac and respiratory adaptation to acute ozone and carbon black exposures: Interstrain variation in mice. *Inhal. Toxicol.* **22**(Suppl 2), 84–94.

Hamade, A. K., Rabold, R., and Tankersley, C. G. (2008). Adverse cardiovascular effects with acute particulate matter and ozone exposures: Interstrain variation in mice. *Environ. Health Perspect.* **116**, 1033–1039.

Harber, P., Muranko, H., Solis, S., Torossian, A., and Merz, B. (2003). Effect of carbon black exposure on respiratory function and symptoms. *J. Occup. Environ. Med.* **45**, 144–155.

Hatch, G. E., McKee, J., Brown, J., McDonnell, W., Seal, E., Soukup, J., Slade, R., Crissman, K., and Devlin, R. (2013). Biomarkers of dose and effect of inhaled ozone in resting versus exercising human subjects: Comparison with resting rats. *Biomark. Insights.* **8**, 53–67.

Hatch, G. E., Slade, R., Harris, L. P., McDonnell, W. F., Devlin, R. B., Koren, H. S., Costa, D. L., and McKee, J. (1994). Ozone dose and effect in humans and rats. A comparison using oxygen-18 labeling and bronchoalveolar lavage. *Am. J. Respir. Crit. Care Med.* **150**, 676–683.

Hathaway, Q. A., Majumder, N., Goldsmith, W. T., Kunovac, A., Pinti, M. V., Harkema, J. R., Castranova, V., Hollander, J. M., and Hussain, S. (2021). Transcriptomics of single dose and repeated carbon black and ozone inhalation co-exposure highlight progressive pulmonary mitochondrial dysfunction. *Part. Fibre Toxicol.* **18**, 44.

Henriquez, A., House, J., Miller, D. B., Snow, S. J., Fisher, A., Ren, H., Schladweiler, M. C., Ledbetter, A. D., Wright, F., and Kodavanti, U. P. (2017). Adrenal-derived stress hormones modulate ozone-

induced lung injury and inflammation. *Toxicol. Appl. Pharmacol.* **329**, 249–258.

Holz, O., Heusser, K., Muller, M., Windt, H., Schwarz, K., Schindler, C., Tank, J., Hohlfeld, J. M., and Jordan, J. (2018). Airway and systemic inflammatory responses to ultrafine carbon black particles and ozone in older healthy subjects. *J. Toxicol. Environ. Health. A* **81**, 576–588.

Hussain, S., Boland, S., Baeza-Squiban, A., Hamel, R., Thomassen, L. C., Martens, J. A., Billon-Galland, M. A., Fleury-Feith, J., Moisan, F., Pairon, J. C., *et al.* (2009). Oxidative stress and proinflammatory effects of carbon black and titanium dioxide nanoparticles: Role of particle surface area and internalized amount. *Toxicology* **260**, 142–149.

Hussain, S., Thomassen, L. C., Ferecatu, I., Borot, M. C., Andreau, K., Martens, J. A., Fleury, J., Baeza-Squiban, A., Marano, F., and Boland, S. (2010). Carbon black and titanium dioxide nanoparticles elicit distinct apoptotic pathways in bronchial epithelial cells. *Part. Fibre Toxicol.* **7**, 10.

Jolliffe, I. T., and Cadima, J. (2016). Principal component analysis: A review and recent developments. *Philos. Trans. A Math. Phys. Eng. Sci.* **374**, 20150202.

Kabesch, M., Schedel, M., Carr, D., Woitsch, B., Fritzsch, C., Weiland, S. K., and von Mutius, E. (2006). IL-4/IL-13 pathway genetics strongly influence serum ige levels and childhood asthma. *J. Allergy Clin. Immunol.* **117**, 269–274.

Kelly, F. J., and Fussell, J. C. (2017). Role of oxidative stress in cardiovascular disease outcomes following exposure to ambient air pollution. *Free Radic. Biol. Med.* **110**, 345–367.

Klimberg, R., and McCullough, B. D. (2016). *Fundamentals of Predictive Analytics with JMP*, 2nd ed. SAS Institute Inc., Cary, NC.

Kuempel, E. D., Tran, C. L., Castranova, V., and Bailer, A. J. (2006). Lung dosimetry and risk assessment of nanoparticles: Evaluating and extending current models in rats and humans. *Inhal. Toxicol.* **18**, 717–724.

Kulkarni, N. S., Prudon, B., Panditi, S. L., Abebe, Y., and Grigg, J. (2005). Carbon loading of alveolar macrophages in adults and children exposed to biomass smoke particles. *Sci. Total Environ.* **345**, 23–30.

Kunovac, A., Hathaway, Q. A., Pinti, M. V., Goldsmith, W. T., Durr, A. J., Fink, G. K., Nurkiewicz, T. R., and Hollander, J. M. (2019). Ros promote epigenetic remodeling and cardiac dysfunction in offspring following maternal engineered nanomaterial (ENM) exposure. *Part. Fibre Toxicol.* **16**, 24.

Li, L., Hamilton, R. F., Jr., and Holian, A. (2000). Protection against ozone-induced pulmonary inflammation and cell death by endotoxin pretreatment in mice: Role of HO-1. *Inhal. Toxicol.* **12**, 1225–1238.

Majumder, N., Goldsmith, W. T., Kodali, V. K., Velayutham, M., Friend, S. A., Khramtsov, V. V., Nurkiewicz, T. R., Erdely, A., Zeidler-Erdely, P. C., Castranova, V., *et al.* (2021a). Oxidant-induced epithelial alarmin pathway mediates lung inflammation and functional decline following ultrafine carbon and ozone inhalation co-exposure. *Redox Biol.* **46**, 102092.

Majumder, N., Velayutham, M., Bitounis, D., Kodali, V. K., Hasan Mazumder, M. H., Amedro, J., Khramtsov, V. V., Erdely, A., Nurkiewicz, T., Demokritou, P., *et al.* (2021b). Oxidized carbon black nanoparticles induce endothelial damage through C-X-C chemokine receptor 3-mediated pathway. *Redox Biol.* **47**, 102161.

Mauderly, J. L., and Samet, J. M. (2009). Is there evidence for synergy among air pollutants in causing health effects? *Environ. Health Persp.* **117**, 1–6.

Maynard, A. D., Aitken, R. J., Butz, T., Colvin, V., Donaldson, K., Oberdorster, G., Philbert, M. A., Ryan, J., Seaton, A., Stone, V., *et al.* (2006). Safe handling of nanotechnology. *Nature* **444**, 267–269.

McKenzie, A. N., Culpepper, J. A., de Waal Malefyt, R., Briere, F., Punnonen, J., Aversa, G., Sato, A., Dang, W., Cocks, B. G., and Menon, S. (1993). Interleukin 13, a T-cell-derived cytokine that regulates human monocyte and B-cell function. *Proc. Natl. Acad. Sci. U S A.* **90**, 3735–3739.

Nadeau, K., McDonald-Hyman, C., Noth, E. M., Pratt, B., Hammond, S. K., Balmes, J., and Tager, I. (2010). Ambient air pollution impairs regulatory T-cell function in asthma. *J. Allergy Clin. Immunol.* **126**, 845–852 e810.

Nurkiewicz, T. R., Porter, D. W., Hubbs, A. F., Cumpston, J. L., Chen, B. T., Frazer, D. G., and Castranova, V. (2008). Nanoparticle inhalation augments particle-dependent systemic microvascular dysfunction. *Part. Fibre Toxicol.* **5**, 1.

O'Brien, N., and Cummins, E. (2010). Ranking initial environmental and human health risk resulting from environmentally relevant nanomaterials. *J. Environ. Sci. Health. A Tox. Hazard. Subst. Environ. Eng.* **45**, 992–1007.

Oberdorster, G., Castranova, V., Asgharian, B., and Sayre, P. (2015). Inhalation exposure to carbon nanotubes (CNT) and carbon nanofibers (CNF): Methodology and dosimetry. *J. Toxicol. Environ. Health. B Crit. Rev.* **18**, 121–212.

Oberdorster, G., Ferin, J., and Lehnert, B. E. (1994). Correlation between particle size, in vivo particle persistence, and lung injury. *Environ. Health Perspect.* **102**(Suppl 5), 173–179.

World Health Organization. (2016). *World Health Statistics 2016: Monitoring Health for the SDGS*. https://www.Who.Int/gho/publications/world_health_statistics/2016/annex_b/en/. Accessed January 14, 2019.

Pacheco, P., White, D., and Sulchek, T. (2013). Effects of microparticle size and fc density on macrophage phagocytosis. *PLoS One* **8**, e60989.

Patel, B., Gupta, N., and Ahsan, F. (2015). Particle engineering to enhance or lessen particle uptake by alveolar macrophages and to influence the therapeutic outcome. *Eur. J. Pharm. Biopharm.* **89**, 163–174.

Patial, S., and Saini, Y. (2020). Lung macrophages: Current understanding of their roles in ozone-induced lung diseases. *Crit. Rev. Toxicol.* **50**, 310–323.

Pink, M., Verma, N., and Schmitz-Spanke, S. (2020). Benchmark dose analyses of toxic endpoints in lung cells provide sensitivity and toxicity ranking across metal oxide nanoparticles and give insights into the mode of action. *Toxicol. Lett.* **331**, 218–226.

Pirela, S. V., Martin, J., Bello, D., and Demokritou, P. (2017). Nanoparticle exposures from nano-enabled toner-based printing equipment and human health: State of science and future research needs. *Crit. Rev. Toxicol.* **47**, 678–704.

Pourazar, J., Frew, A. J., Blomberg, A., Helleday, R., Kelly, F. J., Wilson, S., and Sandstrom, T. (2004). Diesel exhaust exposure enhances the expression of IL-13 in the bronchial epithelium of healthy subjects. *Respir. Med.* **98**, 821–825.

Rattanasom, N., Saowapark, T., and Deeprasertkul, C. (2007). Reinforcement of natural rubber with silica/carbon black hybrid filler. *Polym. Test.* **26**, 369–377.

Rhee, J., Dominici, F., Zanobetti, A., Schwartz, J., Wang, J., Di, Q., and Christiani, D. C. (2018). The impact of long-term exposure to PM2.5 and ozone on the risk of acute respiratory distress syndrome (ARDS) for elderly. *Am. J. Respir. Crit. Care Med.* **197**, A6192.

Riediker, M., Zink, D., Kreyling, W., Oberdorster, G., Elder, A., Graham, U., Lynch, I., Duschl, A., Ichihara, G., Ichihara, S., *et al.*

(2019). Particle toxicology and health—Where are we? *Part. Fibre Toxicol.* **16**, 19.

Ringner, M. (2008). What is principal component analysis? *Nat. Biotechnol.* **26**, 303–304.

Rogers, E. J., Hsieh, S. F., Organti, N., Schmidt, D., and Bello, D. (2008). A high throughput in vitro analytical approach to screen for oxidative stress potential exerted by nanomaterials using a biologically relevant matrix: Human blood serum. *Toxicol. In Vitro* **22**, 1639–1647.

Schulz, D., Severin, Y., Zanotelli, V. R. T., and Bodenmiller, B. (2019). In-depth characterization of monocyte-derived macrophages using a mass cytometry-based phagocytosis assay. *Sci. Rep.* **9**, 1925.

Shehab, M. A., and Pope, F. D. (2019). Effects of short-term exposure to particulate matter air pollution on cognitive performance. *Sci. Rep.* **9**, 8237.

Shin, S. W., Song, I. H., and Um, S. H. (2015). Role of physicochemical properties in nanoparticle toxicity. *Nanomaterials (Basel)* **5**, 1351–1365.

Singh, D., Marrocco, A., Wohlleben, W., Park, H. R., Diwadkar, A. R., Himes, B. E., Lu, Q., Christiani, D. C., and Demokritou, P. (2022). Release of particulate matter from nano-enabled building materials (NEBMS) across their lifecycle: Potential occupational health and safety implications. *J. Hazard. Mater.* **422**, 126771.

Sunil, V. R., Patel-Vayas, K., Shen, J., Laskin, J. D., and Laskin, D. L. (2012). Classical and alternative macrophage activation in the lung following ozone-induced oxidative stress. *Toxicol. Appl. Pharmacol.* **263**, 195–202.

Takahashi, Y., Takahashi, S., Yoshimi, T., Miura, T., Mochitate, K., and Kobayashi, T. (1997). Increases in the mRNA levels of gamma-glutamyltransferase and heme oxygenase-1 in the rat lung after ozone exposure. *Biochem. Pharmacol.* **53**, 1061–1064.

United States Environmental Protection Agency (EPA). (2022). Benchmark Dose Software (BMDS) (Build 3.3; Model Library Version 2022.10) [Computer Software]. Available at: https://www.epa.gov/bmds/download-bmds.

Verma, M., Liu, S., Michalec, L., Sripada, A., Gorska, M. M., and Alam, R. (2018). Experimental asthma persists in IL-33 receptor knockout mice because of the emergence of thymic stromal lymphopoietin-driven IL-9(+) and IL-13(+) type 2 innate lymphoid cell subpopulations. *J. Allergy Clin. Immunol.* **142**, 793–803 e798.

Vranic, S., Boggetto, N., Contremoulins, V., Mornet, S., Reinhardt, N., Marano, F., Baeza-Squiban, A., and Boland, S. (2013). Deciphering the mechanisms of cellular uptake of engineered nanoparticles by accurate evaluation of internalization using imaging flow cytometry. *Part. Fibre Toxicol.* **10**, 2.

Wagner, J. G., Allen, K., Yang, H. Y., Nan, B., Morishita, M., Mukherjee, B., Dvonch, J. T., Spino, C., Fink, G. D., Rajagopalan, S., *et al.* (2014). Cardiovascular depression in rats exposed to inhaled particulate matter and ozone: Effects of diet-induced metabolic syndrome. *Environ. Health Perspect.* **122**, 27–33.

Wang, W., Li, Y., Lv, Z., Chen, Y., Li, Y., Huang, K., Corrigan, C. J., and Ying, S. (2018). Bronchial allergen challenge of patients with atopic asthma triggers an alarmin (IL-33, TSLP, and IL-25) response in the airways epithelium and submucosa. *J. Immunol.* **201**, 2221–2231.

Wei, H., Yuan, W., Yu, H., and Geng, H. (2021). Cytotoxicity induced by fine particulate matter (pm2.5) via mitochondria-mediated apoptosis pathway in rat alveolar macrophages. *Environ. Sci. Pollut. Res. Int.* **28**, 25819–25829.

Weldon, B. A., Griffith, W. C., Workman, T., Scoville, D. K., Kavanagh, T. J., and Faustman, E. M. (2018). In vitro to in vivo benchmark dose comparisons to inform risk assessment of quantum dot nanomaterials. *Wiley Interdiscip. Rev. Nanomed. Nanobiotechnol.* **10**, e1507.

Williams, A. S., Nath, P., Leung, S. Y., Khorasani, N., McKenzie, A. N., Adcock, I. M., and Chung, K. F. (2008). Modulation of ozone-induced airway hyperresponsiveness and inflammation by interleukin-13. *Eur. Respir. J.* **32**, 571–578.

Wilson, A., Reich, B. J., Nolte, C. G., Spero, T. L., Hubbell, B., and Rappold, A. G. (2017). Climate change impacts on projections of excess mortality at 2030 using spatially varying ozone-temperature risk surfaces. *J. Expo. Sci. Environ. Epidemiol.* **27**, 118–124.

Wong, E. M., Walby, W. F., Wilson, D. W., Tablin, F., and Schelegle, E. S. (2018). Ultrafine particulate matter combined with ozone exacerbates lung injury in mature adult rats with cardiovascular disease. *Toxicol. Sci.* **163**, 140–151.

Wottrich, R., Diabate, S., and Krug, H. F. (2004). Biological effects of ultrafine model particles in human macrophages and epithelial cells in mono- and co-culture. *Int. J. Hyg. Environ. Health* **207**, 353–361.

Yang, Q., Chen, Y., Shi, Y., Burnett, R. T., McGrail, K. M., and Krewski, D. (2003). Association between ozone and respiratory admissions among children and the elderly in Vancouver, Canada. *Inhal. Toxicol.* **15**, 1297–1308.

Zhang, R., Dai, Y., Zhang, X., Niu, Y., Meng, T., Li, Y., Duan, H., Bin, P., Ye, M., Jia, X., *et al.* (2014). Reduced pulmonary function and increased pro-inflammatory cytokines in nanoscale carbon black-exposed workers. *Part. Fibre Toxicol.* **11**, 73.

Zheng, R., Tao, L., Jian, H., Chang, Y., Cheng, Y., Feng, Y., and Zhang, H. (2018). Nlrp3 inflammasome activation and lung fibrosis caused by airborne fine particulate matter. *Ecotoxicol. Environ. Saf.* **163**, 612–619.